CHAPTER IV

POLYANILINE NANOFIBERS FOR BIOMEDICAL APPLICATIONS

The present chpater deals with the synthesis and surface functionalization of polyaniline (PAni) nanofibers by glutaraldehyde including their physicochemical and biological characterization. The effects of surface functionalization of PAni nanofibers on their structural, conformational and optical properties have been investigated using TEM, SEM, XRD, I-V characteristics, tensile strength test, TGA, UV-Vis absorption spectroscopy, fluorescence spectroscopy, FT-IR, ^{1}H NMR spectroscopy and contact angle analysis using sessile drop technique. The role of surface functionalization to confer bioactivity to PAni nanofibers has been evaluated in terms of the study of the interaction mechanisms with biomolecules, particularly, aromatic amino acids and several biological charcaterization with living cell systems such as Hemolysis assay with red blood cells (RBCs), MTS proliferation assay and acridine ornage/ethidium bromide (AO/EtBr) staining of MDA-MB-231 cells being cultured on various PAni nanofibers films.

4.1 Introduction

Over the past few decades, one-dimensional (1D) nanostructured materials in the fibrous form have been investigated with considerable interest due to their unique properties and versatile applicability. Researchers across the world have been working in the field of tissue engineering to develop nanofibrous scaffolds for cell attachment and growth from biocompatible materials as nanofibrous materials are capable of providing 3D scaffolds for cellular activities, which are believed to behave like artificial extracellular matrix (ECM) [329]. Moreover, 1D nanostructures as transducers offer ample benefits as novel functional materials for rapid, inexpensive and reliable biosensors for massive parallel sequences analysis of biological activities. Increased surface to volume ratio and facilitation of the electron transport through the bulk of 1D nanomaterials cause a small perturbation by adsorbed charged

chemical/biological molecules on their surface. It significantly affects the charge distribution within the bulk of 1D nanomaterial, enhancing the sensitivity and detection limits [330].

Over the past 25 years, electrically conducting polymers (CPs) have been investigated intensively as novel functional biomaterials due to their ability of highly specific physicochemical and biological functions of practical significance to improve current biomedical devices. Among the illustrative group of these polymeric nanomaterials, 1D nanostructures of polyaniline (PAni) viz., nanofibers, nanotubes, nanowires of PAni deserve a special mention due to its unique properties such as ease of synthesis, low cost, environmental stability, excellent redox stability, high conductivity, and biocompatibility [45, 49]. PAni is not only unique in its molecular structure and doping mechanisms but also has unique optical, electrical and magnetic properties, for which it has found tremendous applications in various fields like supercapacitors [331], electrochromic displays [332], sensors [333], actuators [25], electrorheological materials [334], tissue engineering [123, 157, 229] and controlled release of drugs [335]. Thus, it is quite noticeable that the quest for the area of applications of CPs including PAni has been directed recently towards the diverse biomedical field. However, some serious issues like biocompatibility, biodegradability including unexpected side effects of bioactivity are of critical concern during biomedical application of these materials.

Surface functionalization of nanomaterials has been an extensively employed technique for tailoring the properties of nanomaterials with a view to optimize their functions for certain specific applications. Several properties of nanomaterials such as their biocompatibility, catalytic properties, chemical reactivity and specificity, toxicity etc. can be modulated by functionalizing their surface. Surface functionalized nanomaterials have immense importance in the field of biomedical sciences for applications such as in controlled release and targeted drug delivery [139, 196], biosensors [139, 196], nerve regeneration and tissue engineering scaffolds [139, 196] etc. Surface functionalization of conducting polymer based nanomaterials has been reported by several research groups [139, 234] working primarily in the field of analyte specific biosensors and other biomedical applications. Surface functionalized conducting polymer based nanomaterials provide a suitable substrate for immobilization of enzymes and lead to the fabrication of highly specific biosensors. As such research in this field is primarily focused on studying the effect of surface

functionalization upon the activity of the immobilized enzymes and development of efficient biosensors thereof. However, the effects of surface functionalization upon the structural, optical and conformational properties of the conducting polymer based nanomaterials have not been explicitly investigated and only a handful of reports are available concerning the variations in certain specific properties of PAni bulk after surface functionalization [336, 337]. The variations in the optical properties of the conducting polymers upon surface functionalization with agents such as glutaraldehyde have not been reported at all.

Herein, we have reported large scale production of nanofibers of PAni by dilute polymerization method in a cost effective manner as described by N. R. Chiou *et al.* [267]. We have further functionalized the surface of as-synthesized PAni nanofibers (PNFs) by glutaraldehyde through the incorporation of aldehyde and hydroxyl groups as glutaraldehyde has a higher reactivity towards amine group [301]. The effect of surface functionalization on physicochemical properties of PNFs has been investigated with the help of TEM, SEM, XRD, current-voltage characteristics, TGA, tensile test analyzer, UV-Vis absorption spectroscopy, fluorescence spectroscopy, FT-IR, NMR and contact angle measurement.

In the first embodiment of this chapter, we have described fluorescence enhancement phenomenon of the surface functionalized PAni nanofibers (SF-PNFs) after exposure to aromatic amino acids: tyrosine (Tyr), tryptophan (Trp), and phenylalanine (Phe) through a simple chemical modification technique. It lacks the use of several dyes as in indicator displacement assays (IDAs) and more interestingly, SF-PNFs act as a fluorophore. Remarkable enhancement in fluorescence has been observed after surface functionalization of PNFs. Though photoluminescence of aniline has been found much earlier, photoluminescence of PAni has been reported more elaborately by Shimano *et al* [338]. Normally, the photoluminescence of PAni is quenched due to adjacent quinoid units as reported by Shimano *et al* [338]. The fluorescence of PAni has not been widely reported. Moreover, it has not been used to study the molecular interactions with amino acids till date. The study of variation of fluorescence activity of fluorescence active molecules is an extremely sensitive optical technique for real time monitoring of their interactions with analytes [339, 340]. Fluorescence active molecules used as chemosensors have been explored extensively in diverse fields such as biology [340, 341], medical analysis [340, 342] and environment monitoring [340, 343]. In the present work, we have reported the

fluorescence enhancement of SF-PNFs after treatment with Tyr, Trp, and Phe based on flouorescence resonance energy transfer (FRET) effect between SF-PNFs and the three aforementioned amino acids. The interaction mechanisms have been extensively investigated by FT-IR and ^{1}H NMR techniques and correlated with the results obtained from analysis of fluorescence enhancement effect.

In the second embodiment, the effect of surface functionalization on the cell-biomaterial interaction has been discussed. Herein, the biocompatibility of the materials has been assessed by Hemolysis assay and MTS proliferation assay with MDA-MB-231 cells. Cellular activities such adhesion, spreading and cell morphology have been investigated with the help of fluorescence microscopy after acridine orange/ethidium bromide (AO/EB) staining and SEM.

The schematic illustration of the work carried out is shown in **Figure 4.1**.

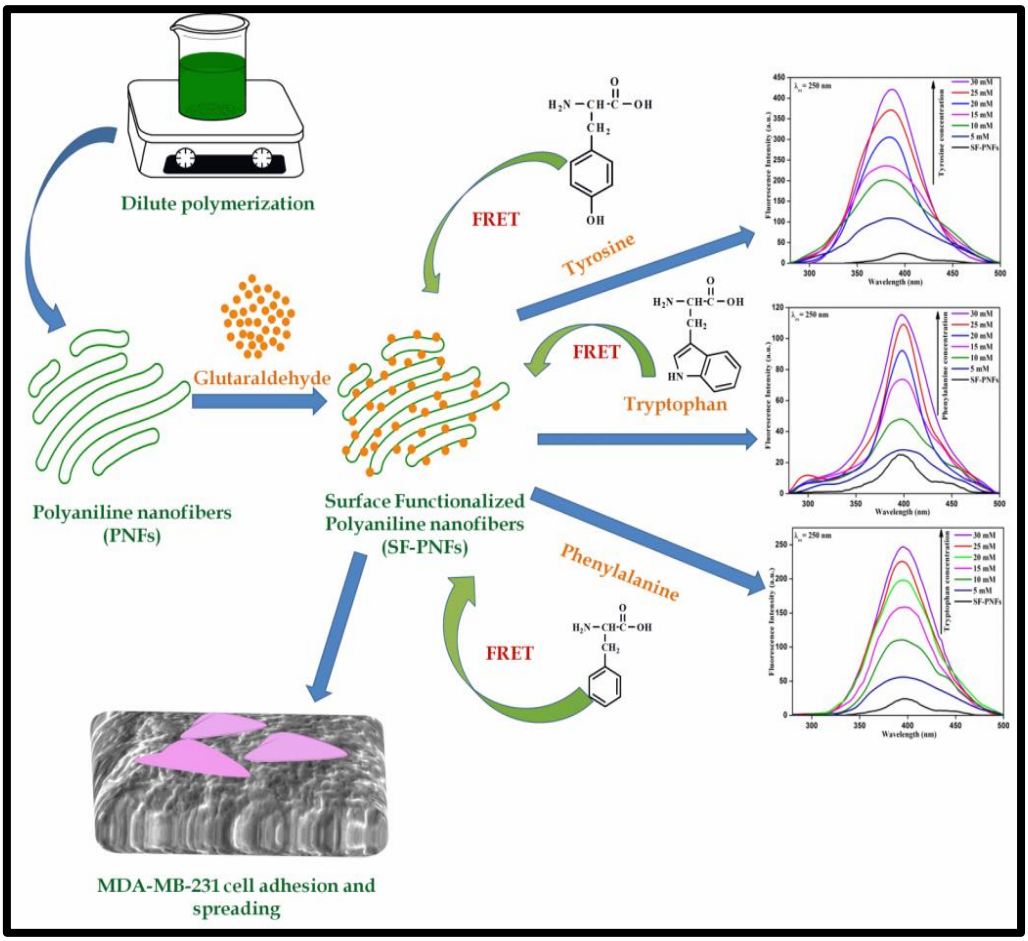

Figure 4.1. Schematic illustration of synthesis of PAni nanofibers (PNFs) by the dilute polymerization technique and surface functionalization by glutaraldehyde for enhanced fluorescence signals in presence of aromatic amino acids (Tyr, Trp and Phe) and for enhanced MDA-MB-231 cell adhesion, spreading and proliferation.

4.2 Physicochemical characterization

4.2.1 Electron microscopy

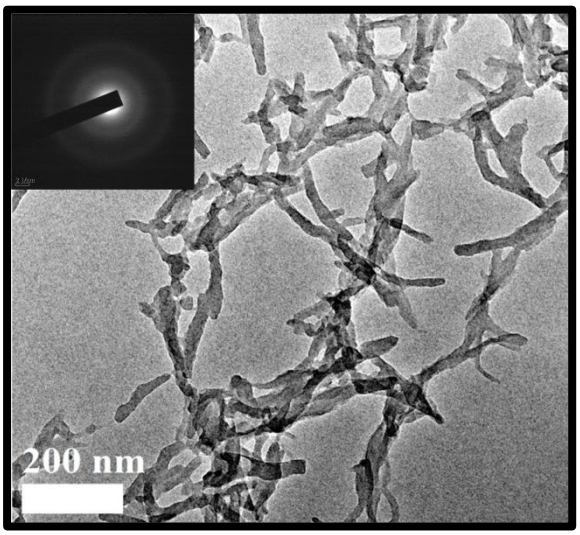

Figure 4.2. Transmission electron micrograph of PAni nanofibers synthesized by dilute polymerization technique. Inset shows the SAED pattern of PAni nanofibers.

Figures 4.2 (a) shows the transmission electron micrograph of hydrochloric acid (HCl) doped PAni nanofibers synthesized by dilute polymerization technique without any secondary overgrowth. The average diameter of the pristine PAni nanofibers has been found to be 36 ± 9 nm. The appearance of only two low intensity diffused rings in the SAED pattern [**Figure 4.2 (c)**] indicates that the PNFs are in amorphous/semi-crystalline phase.

Typical FESEM image of PNFs in powder form in **Figure 4.3 (a)** demonstrates the nanofibrous structures of PAni with interconnected networks produced by dilute polymerization method. The fiber morphology of PNFs film prepared in NMP solution is shown in **Figure 4.3 (b)**. The morphology of the film suggests highly entangled aggregation among the nanofiber networks, which has been confirmed from its stability in solution more than one day [210, 267]. The thickness of the film has been measured to be approximately 30 μm.

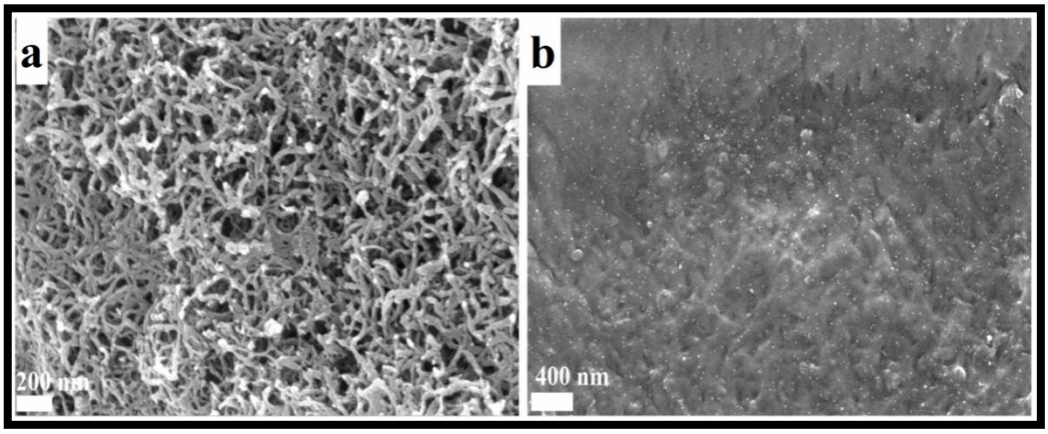

Figure 4.3. Scanning electron micrograph of PAni nanofibers in (a) powder form and (b) film form.

4.2.2 X-ray diffraction analysis

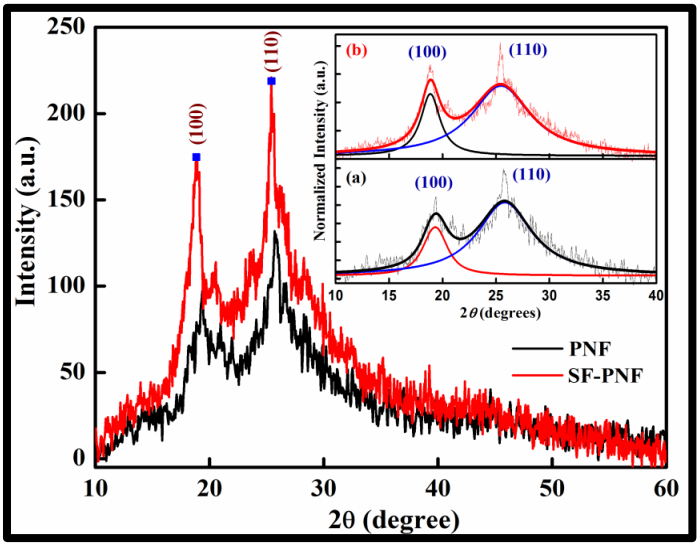

Figure 4.4. X-ray diffraction patterns of PNFs (black) and SF-PNFs (red). Inset shows a Voigtian fit of the x-ray profile that best describes the x-ray pattern for (a) PNFs and (b) SF-PNFs.

The x-ray diffraction patterns of PNFs and SF-PNFs are shown in **Figure 4.4**. Two major reflection peaks are observed for both the samples at 2θ =19° and 25°. In general, the emeraldine salt (ES) form of PAni exists in two crystalline forms ES-I and ES-II depending upon the method adopted for synthesis. The ES-I form is generally considered to have a pseudo-orthorhombic semi-crystalline structure with the unit cell having lattice parameters; a = 4.3 Å, b = 5.9 Å, c = 9.6 Å and a volume of

24.5 Å3 [26]. The major reflections for the ES-I crystalline structure of PAni are observed at 2θ = 15.5°, 20°, 25.5°, 27.6° and 30.2°, which are ascribed to the (010), (100), {(110)}, {(111)}, (020) planes, respectively [344].The two major peaks observed in the x-ray patterns of the pristine PNFs and the SF-PNFs can, therefore, be ascribed to the (100) and (110) reflections. The existence of only two x-ray reflection peaks for the pristine and the SF-PNFs, depicts that the alignment of the PAni chains specifically along the (100) and (110) planes is energetically favourable and surface-functionalization has little effect on its crystalline arrangement. Similar reports have also been observed from the x-ray diffraction patterns of PAni nanofibers synthesized by different techniques [344].

Table 4.1. Characteristics of the X-ray diffraction peaks of PNFs and SF-PNFs corresponding to (100) and (110) reflections.

Sample	**Peaks (hkl)**	***d* (Å)**	***L* (Å)**	**Strain (*e*) (%)**
PNFs	(100)	4.64	19.87	2.78
SF-PNFs		4.83	20.08	2.71
PNFs	(110)	3.56	20.84	2.09
SF-PNFs		3.12	21.31	2.36

Single line approximation has been employed to analyze the diffraction peaks centered at 2θ =19° and 25° and corresponding domain length (L) and strain (ε) have been determined along with d-spacing (**Table 4.1**). Single line approximation enables to extract and analysis of Gaussian (β_G) and Cauchy (β_C) components of an integral breadth of a single Bragg peak corrected for instrumental broadening as discussed in **Chapter III**. It has been found that SF-PNFs have longer domain length (L) and lower strain (ε) than that of PNFs, which suggest improvement in the regular arrangement of the polymer chains due to possible cross-linking between the polymer chains after functionalization with glutaraldehyde.

4.2.3 Current-voltage (I-V) characteristics

The room temperature (300 K) nonlinear *I-V* characteristics of PNFs and SF-PNFs are shown in **Figure 4.5**. Both PNFs and SF-PNFs exhibit nonlinear behavior which is quite symmetric with respect to both the polarity in the applied voltage range of -10 V to +10 V. However, the value of current is slightly higher at a particular voltage for PNFs than that of SF-PNFs. The slight decrease in the value of current for SF-PNFs might be due to loss of π-π conjugation during surface functionalization process.

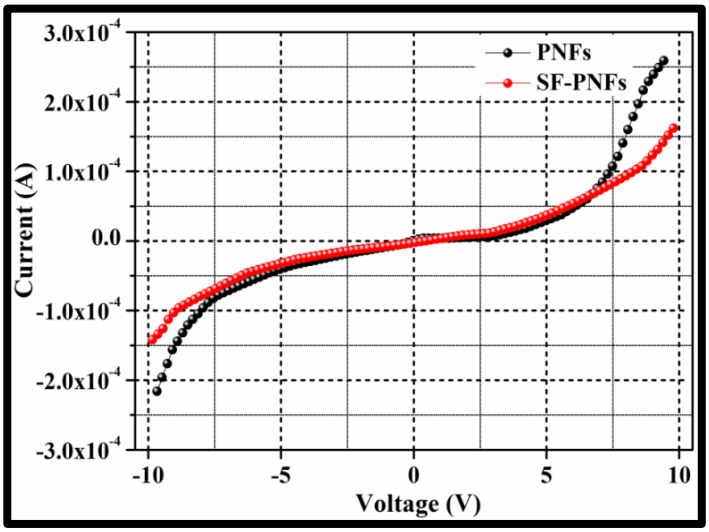

Figure 4.5. Room temperature (300 K) *I-V* characteristics of PNFs and SF-PNFs.

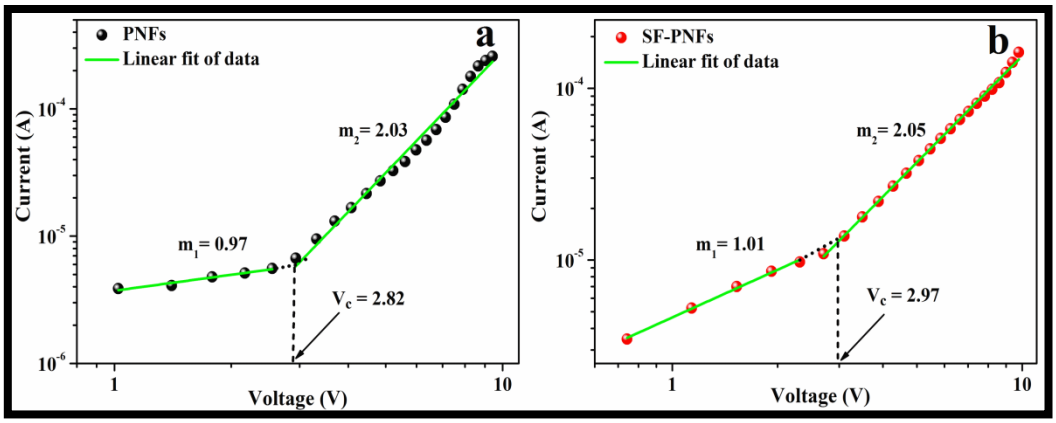

Figure 4.6. Plots of forward I-V data on a log-log scale for (a) PNFs, and (b) SF-PNFs.

The log-log plot of the positive side of the corresponding *I-V* data can provide a better insight into the conduction mechanisms in the materials [345]. The log-log plots show two distinct regions with a gradual transition between the two regions: one in one in the lower voltage region (0<V<3) and other is in the higher voltage region (3<V<10) [**Figure 4.6 (a) & (b)**]. These two distinct linear regions on the log-log plot can be fitted to a power law equation with different exponents, expressed as:

$$I = KV^m \qquad 4.1$$

where K is a constant and m is the exponent, which can be obtained from the slope of the fitted curve. At lower voltage region, the exponent (m_1) is nearly unity and at a higher voltage region, the exponent (m_2) is different from unity as shown in **Figure 4.6 (a) & (b)**. It indicates that at a lower voltage region, the current varies linearly with voltage suggesting the charge transport mechanism is Ohmic, whereas current varies non-linearly at higher voltage region suggesting space charge limited conduction (SCLC). At low voltages, the number of injected electrons is very small as compared to the intrinsic carriers making the charge transport mechanism Ohmic. As the bias voltage is increased above 3 V, a transition from Ohmic to non-Ohmic behaviour takes place, when the density of the injected carriers becomes comparable to the density of the thermally generated free carriers and SCLC occurs. The bias voltage at which the transition from Ohmic to non-Ohmic behaviour occurs is called the critical voltage (V_c) and can be expressed as follows [346]:

$$V_c = \frac{8}{9}\frac{qp_o d^2}{\varepsilon_o \varepsilon_r \theta} \qquad 4.2$$

Where p_o is the density of thermally generated charge carriers, d is the sample thickness, ε_o the permittivity in free space and ε_r is the dielectric constant of the sample. The trap factor is given by, $\theta = p/(p+p_t)$, where p is the density of free charge carriers and p_t is the density of trapped charge carriers, increases due to increase in the free charge carrier density (p) in the sample. The critical voltages (V_c) determined from the log-log plot from the intersection of the two linear lines extended from the linear fit as shown in **Figure 4.6 (a) & (b)** is lower for PNFs than that of SF-PNFs [**Table 4.2**]. The higher value of V_c for SF-PNFs are assigned to the lower density of free charge carriers (p), which results in lower current value at applied bias as compared to PNFs.

The results are further supported by the sheet resistance *(R_s)* values of different PAni nanofibers [**Table 4.2**], which have been calculated using the formula given below [139, 155]:

$$Sheet\ resistance\ (R_s) = R \times \frac{W}{D} \qquad 4.3$$

Where W is the sample width and D is the distance between the two probes of the source meter. R is determined from the inverse of the slope of the *I-V* characteristics. The results shown in **Table 4.2** demonstrate that PNFs has lower surface resistance value as compared to SF-PNFs.

Table 4.2. Calculated sheet resistance (R_s) and critical voltage (V_c) values of PAni nanofibers (PNFs) before and after surface functionalization by glutaraldehyde.

Sample name	Sheet resistance (R_s) Ω.cm	Critical voltage (V_c) V
PNFs	$1.23 \pm 0.48 \times 10^5$	2.82
SF-PNFs	$1.33 \pm 0.55 \times 10^5$	2.97

The non-linear *I-V* characteristics of CP is due to the unique structural features i.e., it contains some ordered conducting regions, which are separated by disorder barriers. This electric field dependent non-linearity of *I-V* curves can be explained with the help of *Kaiser Equation*, which is given by [283],

$$G = \frac{I}{V} = \frac{G_0 \exp(V/V_0)}{1 + h[\exp(V/V_0) - 1]} \qquad 4.4$$

where G_0 is temperature dependence low field ($V \rightarrow 0$) conductance, $h = G_0/G_h$ (h < 1) results in the decrease of *G* below the exponential increase at higher voltages *V* (G_h is the saturated conductance at high field). V_0 is the voltage scale factor that gives an exponential increase in conductance as *V* increases. Since the *I-V* characteristics of PNFs and SF-PNFs are symmetric upon reversal of the voltage direction, the positive side is fitted according to *Kaiser Equation* as shown in **Figure 4.7** and the fitting parameters are presented in **Table 4.3**. It has been observed thatthe value for low field conductance (G_0), voltage scale factor (V_0) and the parameter *h* of PNFs is higher than that of SF-PNFs. The higher value of G_0 for PNFs suggests the easier hopping of

charge carriers throughout the polymer chains, while the voltage scale factor (V_0) also varies in a small range from 2.72 to 2.40, reflecting the smaller change in non-linearities of *I-V* characteristics.

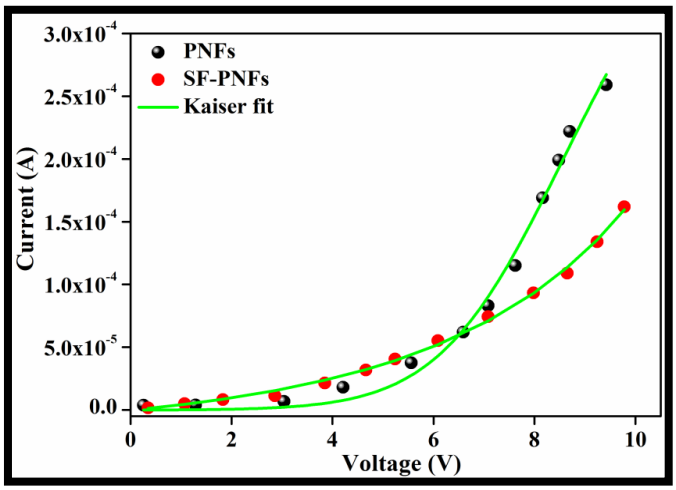

Figure 4.7. Positive sides of *I-V* characteristics of PNFs and SF-PNFs fitted with *Kaiser Equation*.

Table 4.3. Fitting parameters to *Kaiser Equation*for PNFs and SF-PNFs.

Sample	G_o (S)	V_o (V)	h
PNFs	7.59×10^{-5}	2.72	0.032
SF-PNFs	4.61×10^{-5}	2.40	0.023

4.2.4 Mechanical strength test

The scaffolds for supporting cell growth should be mechanically strong enough [121, 180]. The mechanical strength test indicates the strength and elasticity of the film, which can be reflected by the stiffness constant (*E*) and ultimate tensile strength (UTS). The stress *vs.* strain curves and comparison of Young Modulus or stiffness constant (*E*) and ultimate tensile strength (UTS) are presented in **Figure 4.8**. The measured stiffness constant (*E*) and UTS of PNFs have been found to be increased from 39 ± 4 kPa and 579 ± 67 kPa, respectively to 47 ± 5 kPa and 822 ± 84 kPa, respectively, after surface functionalization by glutaraldehyde. The enhanced mechanical properties of PAni nanofibers after surface functionalization are attributed to possible the cross-linking between the polymer chains after surface functionalization and are consistent with the XRD results.

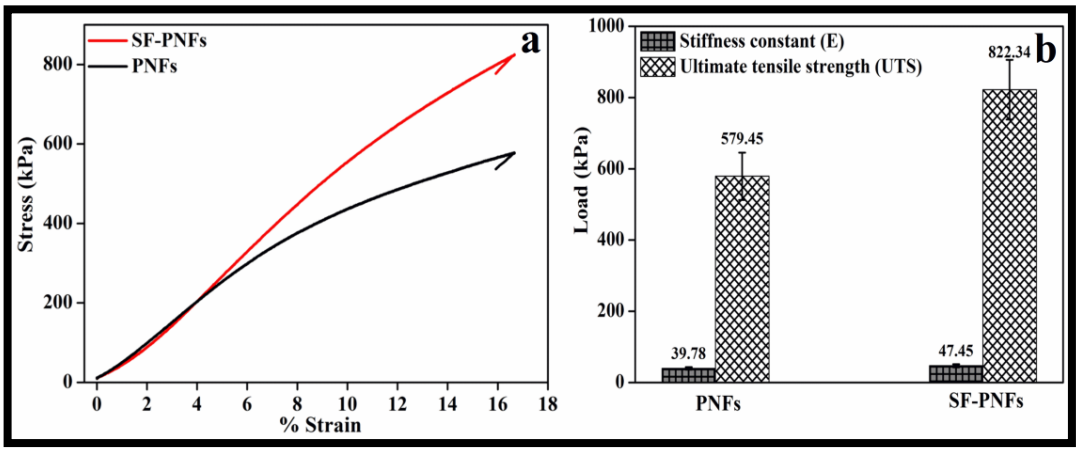

Figure 4.8. (a) Stress *vs* Strain curve of PAni film prepared in NMP before and after surface functionalization; (b) Comparison of Young Modulus or stiffness constant (*E*) and ultimate tensile strength (UTS) of PNFS and SF-PNFs. Data were expressed as Mean ± S.D (n=3).

4.2.5 Stability test

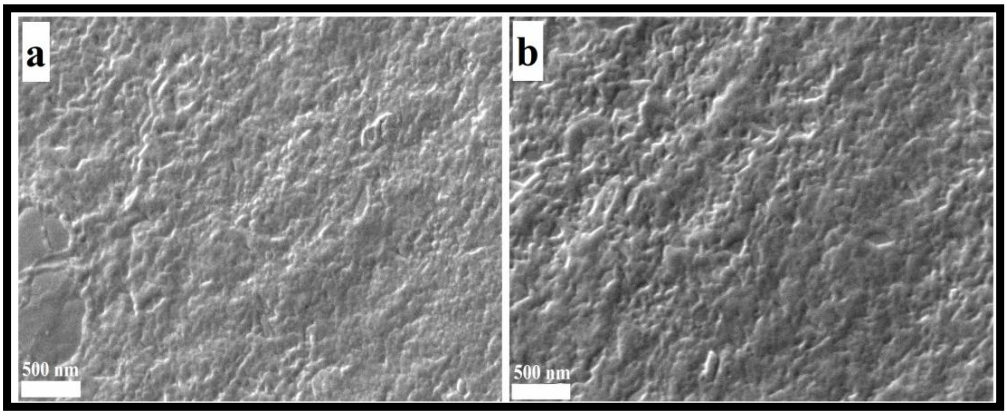

Figure 4.9. Scanning electron micrographs of (a) PNFs, and (b) SF-PNFs recorded after keeping in PBS (pH=7.4) for 30 days (Scale bar = 500 nm).

In order to check the stability of the PAni nanofibers film in physiological condition, both pristine and surface functionalized PAni film were kept in PBS (pH =7.4) for 30 days. To visualize any physical degradation occurs, if any, after keeping in PBS for 30 days, the films were characterized by SEM and to check the conductive properties, the sheet resistances of both the films were measured using source meter. SEM depicts the increase in surface roughness of both PNFs and SF-PNFs after keeping in PBS for 30 days [**Figure 4.9**], when compared to SEM of PNFs before keeping in

PBS [**Figure 4.3 (b)**]. However, the sheet resistances for PNFs and SF-PNFs have not found to change significantly. The sheet resistance of PNFs is increased slightly from $1.23 \pm 0.48 \times 10^5$ Ω.cm to $1.31 \pm 0.61 \times 10^5$ Ω.cm, whereas the sheet resistance of SF-PNFs is increased from $1.33 \pm 0.55 \times 10^5$ Ω.cm to $1.42 \pm 0.72 \times 10^5$ Ω.cm, after treatment with PBS. The results suggest that PAni films before and after surface functionalization are stable enough in physiological condition due to the non-degradable nature of PAni, which indicates the potential of these nanofibers as a conductive scaffold for neural tissue engineering. It has been found that the percentage of weight loss of the non-functionalized and the surface functionalized PAni films are as 1.23% and 1.09% respectively, indicating their non-degradable nature.

4.2.6 Thermogravimetric analysis (TGA)

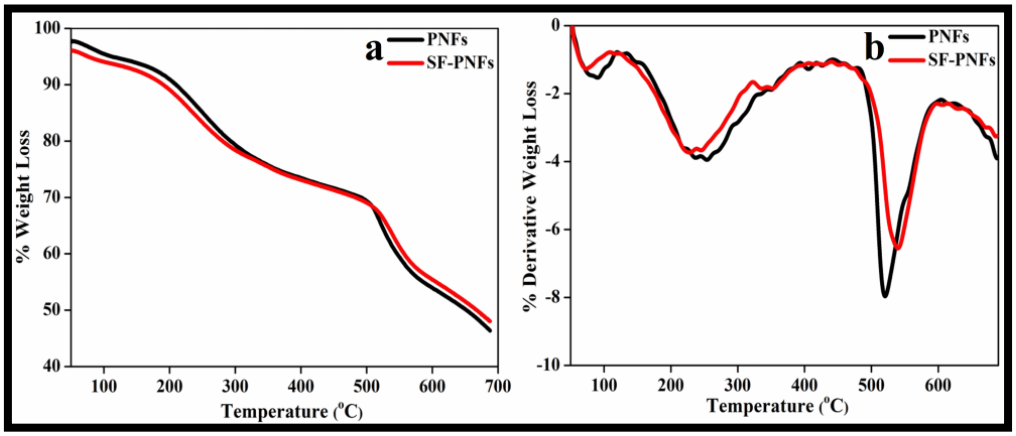

Figure 4.10. (a) TGA thermograms and (b) DTG plots of PNFs and SF-PNFs.

The thermal behaviour of PNFs and SF-PNFs has been investigated at a heating rate of 30°C/min under nitrogen atmosphere. The TGA thermograms and DTG plots of PNFs and SF-PNFs are shown in **Figure 4.10 (a) and (b)**. The weight loss below 100°C in both PNFs and SF-PNFs is attributed to the elimination of small amount of moisture [347]. Approximately, 5% weight loss occurs at 72°C for SF-PNFs and at 92°C for PNFs. The reason for the higher weight loss at lower temperature in SF-PNFs than PNFs can be attributed to the presence of free glutaraldehyde molecules in addition to moisture on the surface of PNFs after functionalization. The weight loss observed around 250°C is attributed to the evaporation of NMP solvent [348]. The

thermogram of SF-PNFs shows a weight loss in the range of 335-355°C, which cannot be detected in PNFs. This may be due to the covalently bonded glutaraldehyde molecules in PAni chain. Before functionalization, PAni film shows a weight loss 23-25% and after surface functionalization with glutaraldehyde, it shows a weight loss of about 24-26% in the range of 335-355°C. Thereby, the estimated amount of actual glutaraldehyde incorporated onto the surface of PAni through covalent bonding is to be of about 1%. The major degradation temperature for the polymer backbone has been observed to be shifted from 519°C to 538°C after surface functionalization. This may be due to the different chemical structure of benzenoid and quinoid units in PAni chains after functionalization [348]. It is further clear from **Figure 4.10 (a)** that PNFs lose 36% of their weight at 519°C, while SF-PNFs lose 37% of their weight at 538°C. It reveals that the weight loss corresponding to the PAni chains in SF-PNFs is slightly slower than that of PNFs, which leads to the improved thermal stability of the PAni after surface functionalization.

4.2.7 FT-IR spectroscopy

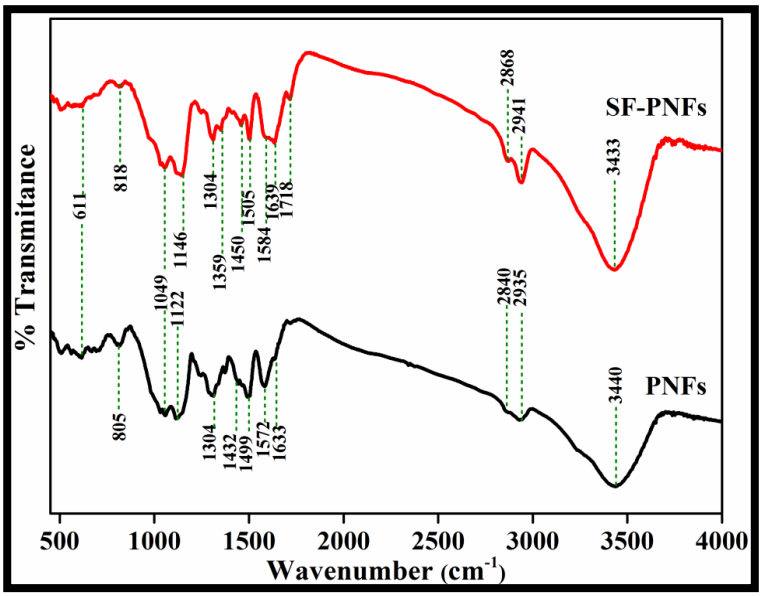

Figure 4.11. Vibrational spectra of PNFs (black) and SF-PNFs (red) showing incorporation of polar functional hydroxyl (-OH) and aldehyde (-CHO) groups.

The recorded FT-IR spectrum of PNFs (black) in **Figure 4.11** shows characteristics vibrational bands for PAni, whereas the FT-IR spectrum of SF-PNFs (red) contains some new bands in addition to shifting and broadening of some characteristics

vibrational bands of PAni. The broad vibrational bands around 3440 cm^{-1} of PNFs and 3433 cm^{-1} of SF-PNFs are assigned to the N-H stretching vibrations of primary and secondary amines attached to benzenoid units of PAni [349-351]. The enhancement in intensity and shifting of this band to higher wavenumber for SF-PNFs can be ascribed to the overlapping of O-H stretching vibration of cyclic hemiacetal and oligomeric form of glutaraldehyde in SF-PNFs [351]. The lowering of N-H stretching wavenumber in SF-PNFs reveals the intermolecular hydrogen bonding between amine and hydroxyl group [352].The absorption bands in the 2868-2935 cm^{-1} region of PAni due to aromatic C-H stretching shifts to 2861-2927 cm^{-1} in SF-PNFs with an increase in intensity [349-351]. It indicates the overlapping O-H bending vibration of cyclic hemiacetal or/and oligomeric form of glutaraldehyde [351]. A sharp peak with medium intensity, unlike the pristine PNFs, at 1720 cm^{-1} for SF-PNFs attributed to C=O stretching vibration of non conjugated aldehyde confirms the presence of monomeric glutaraldehyde [351]. The weak absorption band at 1636 cm^{-1} of PNFs is attributed to C=N aromatic stretching vibrations in quinoid units, which converts into a strong and broad one at 1639 cm^{-1} in SF-PNFs. This can be simultaneously attributed to C=O stretching vibrations in amide bond and C=N stretching vibrations in Schiff base formed between aldehyde group of monomeric glutaraldehyde and the primary amine of PNFs [351, 352]. The strong absorption bands, appearing at 1582 cm^{-1} in the vibration spectra of PNFs and SF-PNFs are assigned to C=C stretching vibration of quinoid units of PAni [349-351]. The appearance of vibrational bands in the region 1442-1502 cm^{-1} PNFs is due to characteristics C=C stretching vibrations of benzenoid units in PAni, however, it shifts to 1504 cm^{-1} for SF-PNFs with relatively higher intensity. The weak band at 1234 cm^{-1} in PNFs corresponding to various stretching and bending vibrations of C-C bond, has been observed to be upshifted to 1240 cm^{-1} in SF-PNFs. The strong peak at 1306 cm^{-1} along with a small shoulder peak at 1370 cm^{-1} in the FT-IR spectrum of PNFs belongs to the characteristic of C-N stretching vibrations, related to aromatic amine [350, 351]. The sharp splitting and shifting of these two peaks in SF-PNFs to lower wavenumber region 1304-1354 cm^{-1} with increase in intensity indicates possible interaction of cyclic hemiacetal forms of glutaraldehyde with amine and imine sites of PNFs through covalent bonding. The intense bands at 1054-1114 cm^{-1} in PNFs, associated with C-H in plane bending vibrations, shift to 1048-1145 cm^{-1} region [349-351]. This change can be attributed due to overlapping of O-H bending vibrations. The weak absorption band seen at 818

cm^{-1} of PNFs shifts to lower frequency region for SF-PNFs into 812 cm^{-1} indicating an increase of the degree of oxidation of para-disubstituted benzene after functionalization [349, 352].

4.2.8 ^{1}H NMR spectroscopy

In ^{1}H NMR spectrum of PNFs in deuterated dimethyl sulfoxide (DMSO) as shown in **Figure 4.12**, the strongest peak broad is observed centered at 6.9 ppm is due to the protons in the benzenoid units [353-355]. A doublet of unequal strength observed at 7.6-7.8 ppm is associated with disubstituted phenylene i.e., quinoid units [353, 354]. The relatively higher peak area corresponding to the protons in the benzenoid units than the protons in the quinoid units indicates the higher number of benzenoid units than that of the quinoid units in the polymer chain, which is also suggested by UV-visible and photoluminescence results as discussed in the later sections.

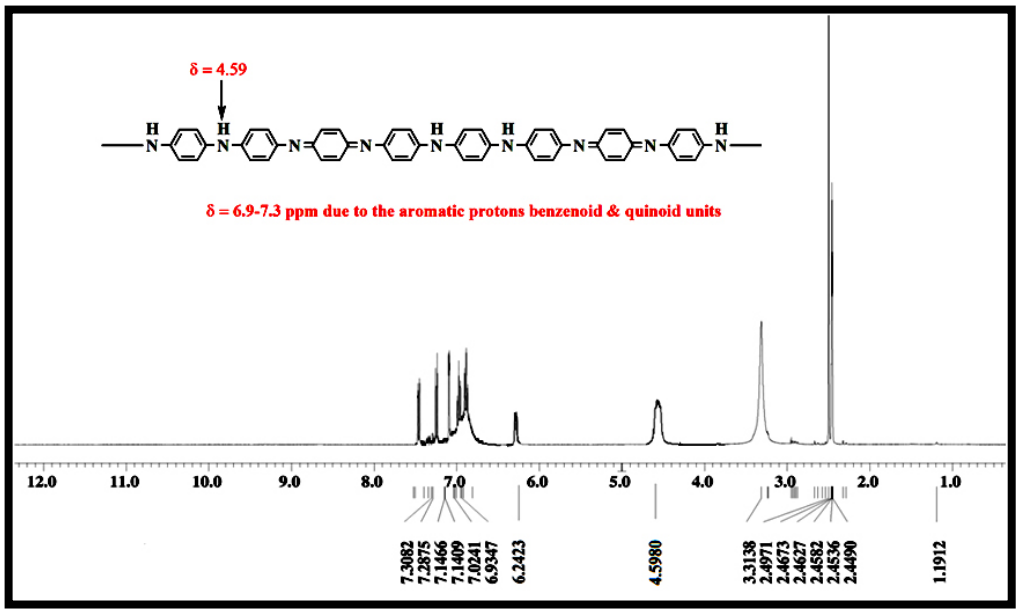

Figure 4.12. ^{1}H NMR spectrum showing the characteristics peaks of PNFs. Observed peaks are assigned by labelling the various protons in different chemical environment in predicted chemical structure of the polymer.

A sharp peak of medium strength appeared at 6.2 ppm corresponds to end primary amine group attached with benzene ring adjacent to a secondary amine which is also attached with another benzene unit [353-355]. The characteristic peak of unprotonated secondary amine (-NH) within the polymer chain appears at 4.6 ppm [354-355].

Generally, ES form of PAni shows three equally spaced peaks of equal strength in the region 6.9-7.3 ppm in ^{1}H NMR spectrum as a result of protonated -NH resonance due to the ^{14}N with unit spin which makes the proton attached to it split into three lines as reported earlier [354]. It is possible only if proton exchange process is much slower. It has been also reported that proton exchange process becomes slower in ammonium ion [352]. Moreover, another weak peak is observed for ES form of PAni due to hydrogen bonding between water and H-N^{+} [354]. Ultimately, the absence of the sharp and equidistant triplet of equal strength in the range 6.9-7.3 ppm and the single small peak in the region 8 ppm reveals that the PNFs are in emaraldine base (EB) form, which supports our earlier reported result.

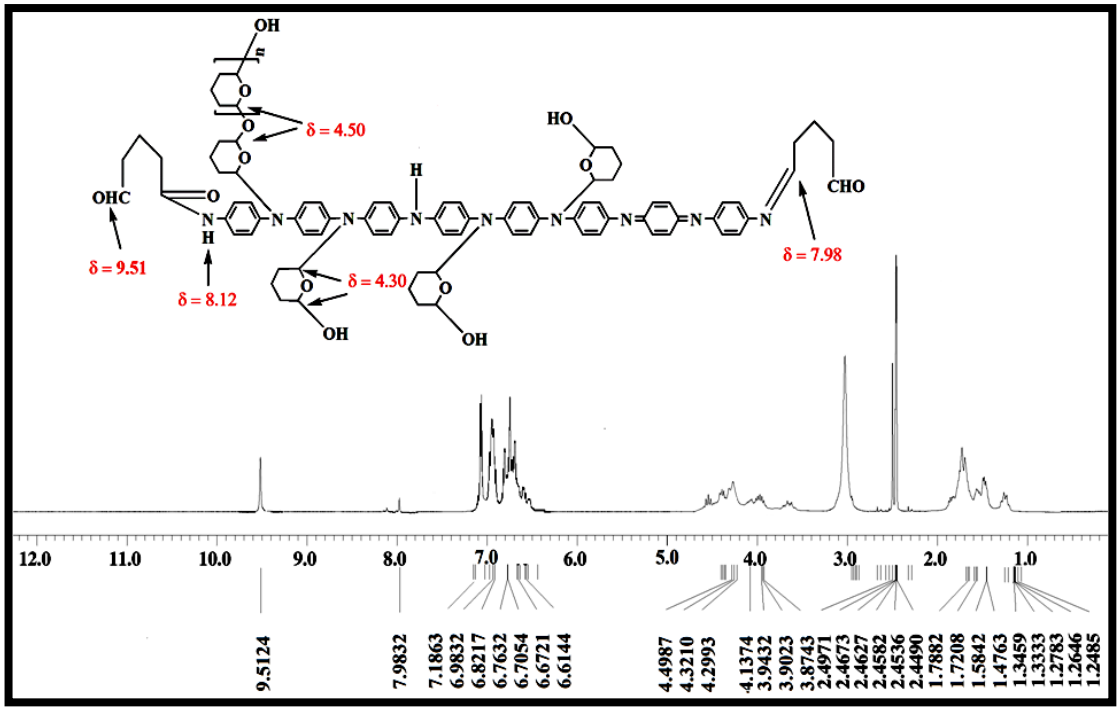

Figure 4.13. ^{1}H NMR spectrum of SF-PNFs showing the chemical shift value after incorporation of hydroxyl (-OH) and aldehyde (-CHO) functional groups. Observed peaks are assigned by labelling with the help of predicted chemical structure of the polymer.

It has been observed that the ^{1}H NMR signals due to the aromatic protons of PAni chain after surface functionalization shift towards upfield as compared to pristine suggesting deprotonation of PAni chain after functionalization with glutaraldehyde is shown in **Figure 4.13** [354]. Interestingly, the intensity of the signal at 4.6 ppm

associated with unprotonated secondary amine (-NH) is found to be decreased in SF-PNFs as compared to pristine PNFs, which indirectly indicates the oxidation (loss of hydrogen as shown in **Figure 4.15**) of the secondary amine within the polymer chain during the conjugation with hydroxyl (in case of cyclic hemiacetal) or aldehyde (in case of monomeric form) group of glutaraldehyde. Conjugation of cyclic hemiacetal or/and oligomeric form of glutaraldehyde is also supported by the appearance of two prominent NMR signals in the range 4.7-4.9 ppm in the ^{1}H NMR spectrum of SF-PNFs. These new peaks are attributed to the protons in cyclic hemiacetal or/and oligomeric form of glutaraldehyde which is in close environment to oxygen as shown in predicted chemical structure of SF-PNFs in **Figure 4.13**. More interestingly, the signals assigned to end primary amine group attached to benzenoid unit at 6.2 ppm in PNFs are found to be completely disappeared after surface functionalization. It is due to the fact that glutaraldehyde has significantly higher reactivity towards primary amine. This confirms that primary amine groups present at the end terminals of PAni have been utilized in Schiff base formation during the conjugation with monomeric glutaraldehyde, which is shown with detailed reaction mechanisms in **Figure 4.15**. The appearance of another new peak at 9.7 ppm in SF-PNFs attributed to aldehyde (-CHO) group, further confirms the presence of monomeric glutaraldehyde.

4.2.9 UV-visible absorption spectroscopy

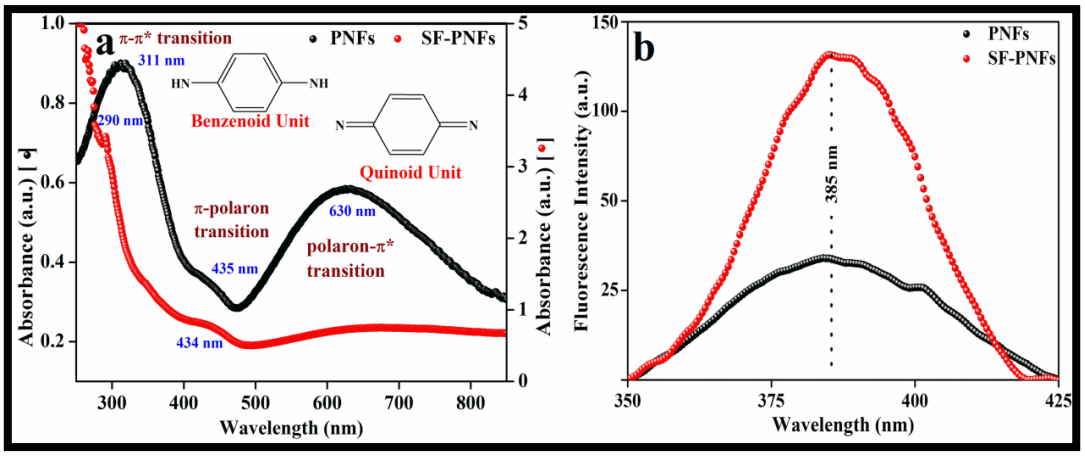

Figure 4.14. (a) UV-visible absorption spectra (b) emission spectra of PNFs and SF-PNFs in 0.1M PBS at p^{H}=7.4 (λ_{ex}=280 nm).

Figure 4.14 (a) shows the UV-Visible absorption spectra of the pristine PNFs and SF-PNFs in 0.1M PBS. PAni shows a strong coupling between its electronic structure and geometric features such as the polymer chain conformation as proved by experimental as well as theoretical studies [356]. Particularly the phenyl and phenyl/quinoid torsional angles along the polymer chain play a significant role in determining its electronic structure and thus affect its absorption spectra. The polymer chain conformation as well as the conjugation length, therefore, determines the position and intensity of the absorption bands for PAni [357, 358].

Three absorption bands centred at 311 nm, 432 nm and 630 nm are observed in the absorption spectra of pristine. PAni bulk exhibits a peak centred at 330 nm associated with the π–π* band transitions, i.e., electronic transitions from the HOMO to LUMO and gives an idea of the band gap of the polymer. This peak appears in the absorption spectra of both the emeraldine base (EB) and emeraldine salt (ES) forms of PAni [356]. This absorption band has also been associated with the excitation of the benzenoid units in the polymer chain. The band transition peak for the pristine PNFs has been observed at 311 nm, which is slightly blue shifted compared to the normally observed band transition peak at 330 nm peak for bulk PAni. This blue shift is quite natural for PNFs, since reduction in particle size leads to the increase in the energy band gap and as such the absorption peak shifts to lower wavelengths. Similar variations in the absorption spectra of PAni in its nanofiber form have been reported earlier [356-358]. The band transition peak for the SF-PNFs is however, observed at 291 nm.

Figure 4.14 (a) also reveals another peak at 630 nm for the pristine which is generally observed in the insulating EB form of the polymer ascribed to a local charge transfer between a quinoid ring and the adjacent imine-phenyl-amine units giving rise to an intramolecular charge transfer exciton [356, 359]. The ES on the other hand is characterized by the formation of a polaron band deep inside the band gap of the polymer [356, 359]. The excitation of this polaron lattice gives rise to two visible region bands in the absorption spectra of ES form of PAni. The 630 nm band that arises due to the quinoid excitation disappears and two new visible region bands due to the excitation of the polaron bands are observed; one at 430 nm and a long tail centred at 800 nm. Specifically, the 430 nm band is associated with the π-polaron band transitions, while the 800 nm peak is due to the polaron-π* band transitions.

From the **Figure 4.14 (a)**, it is evident that the pristine PAni nanofibers exhibit bands both at 430 nm and 630 nm indicating that the pristine PNFs are in a state between the EB and ES form. The relative intensities of the peak, however, suggest that the quinoid units are dominating as compared to the benzenoid units in pristine.

For the SF-PNFs, however, besides the peak associated with the band transition at 311 nm, observed in case of pristine, has been shifted towards lower wavelength (~290 nm) region of the absorption spectra, two other peaks are observed; one at 430 nm, which is a signature of the ES salt form and another peak centered at 800 nm attributed to the ES form of PAni. The peak at 800 nm appears when the PAni chains adopt a "compact coil" conformation. However, when an "extended coil" conformation is adopted, this localized polaron band is replaced by a broad, strong free carrier tail in the NIR, with λ_{max} red shifted to 1500-2500 nm. The delocalization of the polaron along the PAni chains in this "extended coil" conformation results in a much enhanced electrical conductivity [356-359]. This indicates that although dilute polymerization produces PAni nanofibers in an intermediate state between the EB and ES forms, surface functionalization with glutaraldehyde converts it into more of its ES form through reduction of quinoid units resulting in greater number of benzenoid units in the chain as is evident from the absorption spectroscopy. This modification can be ascribed to the interaction between the amine and imine group of PAni chain and glutaraldehyde as glutaraldehyde has a high degree of reactivity towards amine group, which is in agreement with FT-IR and ^{1}H NMR results discussed above. However, the *I-V* characteristics results show no significant change in conductive properties of PAni nanofibers after functionalization. UV-Vis absorption study has been carried out in solution phase, while *I-V* characteristics have been carried out in film form. This may be the reason of the difference in the results obtained by these two characterization techniques.

4.2.10 Fluorescence spectroscopy

Figure 4.14 (b) shows the fluorescence spectra of the pristine and glutaraldehyde functionalized PNFs along with that for aqueous solution of glutaraldehyde for an excitation wavelength of 280 nm. Both PNFs and SF-PNFs exhibit a distinct photoluminescence peak at 385 nm. However, the intensity of the peak of SF-PNFs is observed to be higher than the PNFs. Leucoemeraldine base (LEB) form of PAni

exhibits a photoluminescence peak at 400 nm associated with the fully reduced benzenoid unit and the photoluminescence of PAni is quenched if the (fully reduced) benzenoid unit is situated adjacent to a (fully oxidized) quinoid unit [338]. The disappearance of photoluminescence in EB form of PAni is generally attributed to the fact that the benzenoid and quinoid units in emeraldine base were believed to be located adjacent to each other. Here, we have observed photoluminescence in both PNFs and SF-PNFs, though UV-visible absorption spectroscopy suggests that both the samples are in intermediate state of EB and ES form. This contradiction can be resolved on the basis of the explanations proposed by Shimano *et al.* taking into account a dynamic block co-polymeric structure of PAni with two benzenoid units adjacent to a single quinoid unit [338]. Furthermore, the photoluminescence of PAni in LEB form was reported to be enhanced. We have also found enhancement in fluorescence intensity after surface functionalization at 385 nm assigned to the π–π* transition of the benzenoid unit. During the transformation of EB to ES, the peak around 400 nm begins to disappear while the peak around 470 nm begins to appear prominently [338]. But, no such kind of transformation is observed in our case except the fluorescence enhancement at 385 nm, suggesting that though the PAni nanofibers are initially in EB form, surface functionalization at neutral pH value reduce the quinoid units into benzenoid like structures. The enhancement in the fluorescence intensity after surface functionalization is ascribed to increased number of benzenoid like units in the polymer chain due to partial reduction at the imine sites as well as incorporation of functional oxygenated species like CHO, OH in the polymer by functionalization of glutaraldehyde through grafting. The partial conversion of quinoid units into benzenoid units indicates the partial transformation of EB form to the LB form of PAni, which has also been revealed by the suppression of the peak at 600 nm associated with quinoid units observed in UV-Visible spectra analysis. This observation reveals that there is no probability of formation of polaron band in SF-PNFs giving only π–π^*transition. It is well reported that fluorescence is more probable if the lowest energy transition is for π^*–π than n-π^* as the molar absorptivity of the former is greater than that of the latter [360-362].

4.3 Surface functionalization induced variation in redox state of PAni

The effect of functionalization of PNFs on optical properties in acidic condition has been reported in our published report [363]. However, the effect is slightly different neutral condition as we have studied so far.

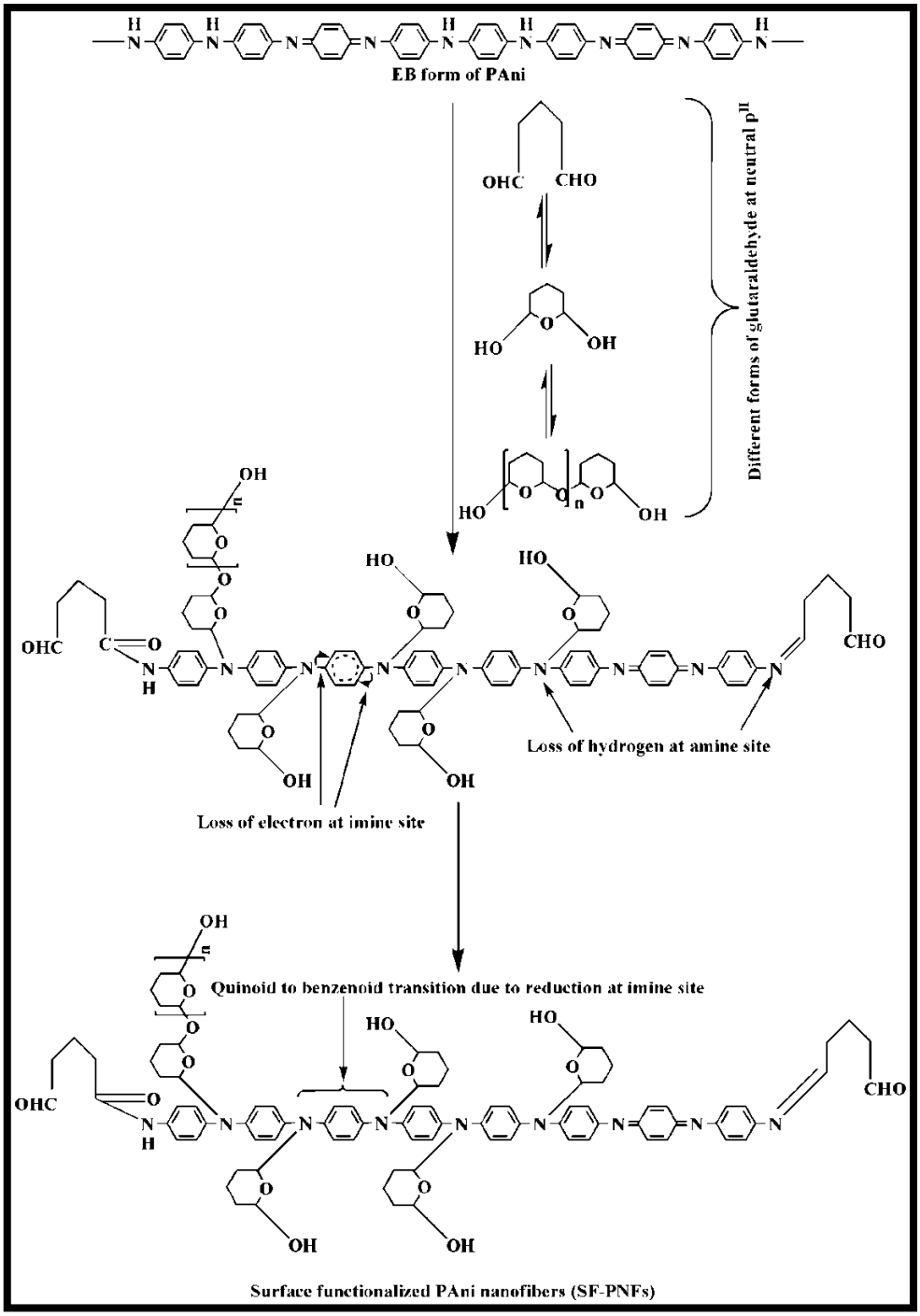

Figure 4.15. Scheme of possible functionalization mechanisms of PNFs by three different forms of glutaraldehyde showing quinoid to benzenoid transformation in the polymer chain.

It is in the sense that surface functionalization in acidic condition revealed a transition of EB towards ES form of PAni, while in the present work it is observed that surface functionalization causes a partial transition of EB form of PAni into LB form. Considering the results obtained so far by UV-visible, photoluminescence, FT-IR and 1H NMR spectroscopy, we have proposed a detailed functionalization mechanism of PNFs by glutaraldehyde. The possible functionalization mechanism is shown in **Figure 4.15** and tries to cover all the outcomes obtained till now. Based upon the experimental results from FTIR, UV-Visible and fluorescence spectroscopy we have proposed possible reaction mechanisms for surface functionalization of the PAni nanofibers with glutaraldehyde, which can explain the observed changes in the optical properties of the SF-PNFs. Functionalization mechanism of PNFs depends on different chemical structure of glutaraldehyde in aqueous solution. Isabelle Migneault *et al.* [301] reported different forms of glutaraldehyde in aqueous solution depending on the pH of the solution. In our case, the pH of the colloidal solution of the polyaniline nanofibers was measured to be around 7. Hardy *et al.* [301 and refs therein] and Korn *et al.* [301 and refs therein] proposed that under this condition (at low pH), glutaraldehyde can exist in aqueous solution in a mixture of three forms-monomeric form, cyclic hemiacetal and polymeric form i.e.; cyclic hemiacetal oligomer as shown in the different forms of glutaraldehyde in **Figure 4.15.** Based on these considerations, we have presented a reaction mechanism of the three forms of glutaraldehyde with PAni, which ultimately reduce the quinoid units and thereby, converts it to benzenoid unit [**Figure 4.15**] [363].

4.4 Enhancement in surface free energy and surface polarity after surface functionalization

It was reported earlier that surface properties of a material like wettability which is an important phenomenon for binding or adherence between two materials, can be evaluated by calculating surface energy of that material using contact angle values of different polar and apolar test liquids on it [364, 365]. Usually, the high energy surfaces due to nature of the chemical bonds (viz. covalent, ionic) hold them together, possess higher wettability. Thus, the presence of chemical groups present on the surface of a material defines the wettability, which is one of the most prerequisite parameters correlated with cell-biomaterial interfacial interactions. So far as, we have

demonstrated directly the incorporation polar functional groups onto the surface of PNFs with the help of FT-IR and NMR spectroscopy, there are no such direct method to calculate the total surface energy or surface tension except some indirect or semi-empirical methods.

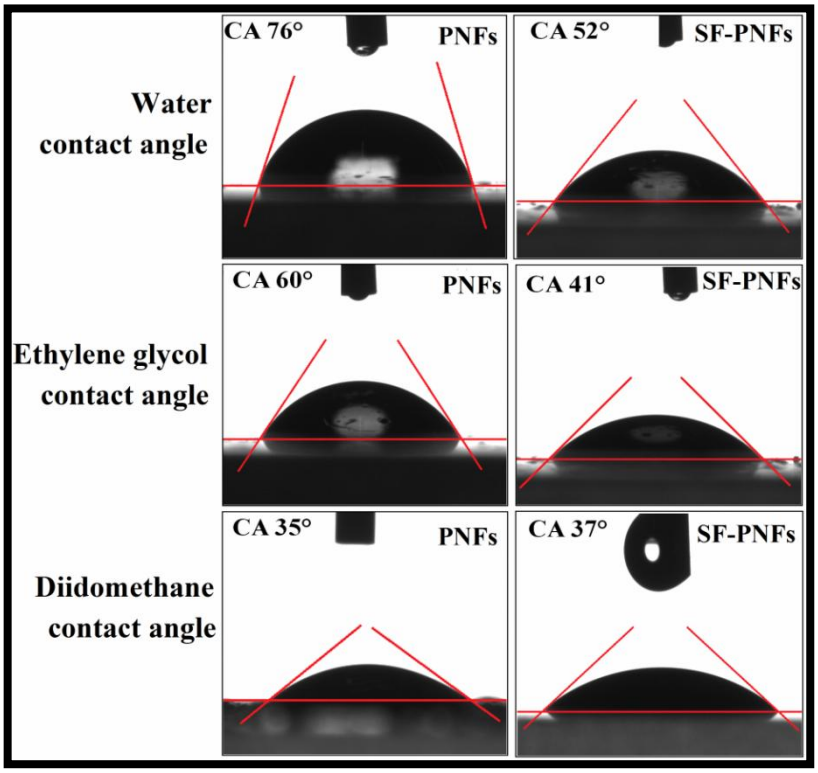

Figure 4.16. Representative images of contact angle measurement using three different liquids (water and ethylene glycol as polar liquids and diiodomethane as non polar liquid) on film of PNFs and SF-PNFs.

Table 4.4. Average contact angle values ± S.D. of water, ethylene glycol and diiodomethane on pristine and surface functionalized PAni films.

Material	Water Contact angle (°)	Ethylene Glycol Contact angle (°)	Diiodomethane Contact angle (°)
PNFs	76.2 ± 0.8	60.2 ± 0.2	34.6 ± 1.3
SF-PNFs	52.1 ± 0.3	40.7 ± 0.8	37.2 ± 1.8

Contact angle values of PNFs before and after surface functionalization with glutaraldehyde with three different test liquids are shown in **Table 4.4**. Decrease in

water contact angle value upto 52.1° after functionalization reveals the improved wettability of the material surface.

Table 4.5: Surface energy and its components calculated by the OWRK method taking water and diiodomethane as probe liquids. Data are Mean ± S.D.

Material	OWRK method			
	γ_s^d mNm^{-1}	γ_s^p mNm^{-1}	γ_s mNm^{-1}	% Polarity
PNFs	42.19 ± 1.67	4.29 ± 0.98	46.48 ± 2.34	9.30 ± 1.08
SF-PNFs	40.96 ± 2.01	12.19 ± 1.12	53.15± 1.88	22.93 ± 2.35

Table 4.6. Surface energy and its components calculated by AB method taking water, ethylene glycol and diiodomethane probe liquids. Data are Mean ± S.D.

Material	AB method				
	γ_s^{LW} mNm^{-1}	γ_s^- mNm^{-1}	$\gamma_s^{\mp}$ mNm^{-1}	γ_s mNm^{-1}	% Polarity
PNFs	42.19 ± 1.67	13.50± 1.39	0.73± 0.27	48.46± 3.07	12.93± 0.89
SF-PNFs	40.96 ± 2.01	32.87± 2.23	0.64± 0.11	50.13± 4.28	18.30± 1.45

The total Surface energy (γ_s) along with its dispersive (γ_s^d) and polar (γ_s^p)components using two test liquids water/ethylene glycol and diiodomethane by OWRK method have been presented in **Table 4.5**. It was established earlier that increase in the value of polar component of surface energy indicates the increase in the concentration of polar groups on the polymer surface [366]. It has been found that the total surface energy value after functionalization is increased significantly from 46.48 $mNm^{-1}$to 53.15 mNm^{-1} .This reveals enhancement in wettability of the functionalized surface. Also, the increase in polar component (12.19 mNm^{-1}) after surface functionalization has proved indirectly the incorporation of polar functional groups like hydroxyl and aldehyde groups through glutaraldehyde onto the surface of PNFs. It is also to be noted that the presence of a small value of polar component of surface energy but not readily negligible, in case of pristine PNFs can be assigned to the available polar groups like primary and secondary amines in the polymer chains and thereby hydrophilicity of the surface is enhanced.

Furthermore, surface energy calculations of PNFs before and after surface functionalization are also performed by AB method using three test liquids: water, ethylene glycol and diiodomethane and presented in **Table 4.6**. One of the major advantages of this method over the earlier one is that it can provide a complete scenario along with acidic and basic character of the surface beyond the total surface energy and dispersive-polar components. In fact, the "polar" term designate three classes of compound viz. hydrogen bonding compounds, dipolar compounds and the compounds that interact with Lewis acid and base [366, 367]. This AB method reported by Van Oss et al., distinguishes this acid base interactions as a component of surface energy denoted by γ^{AB}. The results obtained from this method differ slightly from OWRK method though the results of both the methods can be correlated as the enhancement in total surface energy and its polar component can be observed in both cases. As seen from Table III, the Lifshitz-Van der Waals components of PNFs after surface functionalization significantly decreased to 40.96 mNm^{-1} from 42.19 mNm^{-1}, which is also evident from OWRK method. But, the most important observation is the increase in acid-base components of surface energy after surface functionalization which ultimately points to the improved hydrophilicity of the surface. To speak more specifically, the Lewis base component (γ_s^-) of SF-PNFs is enhanced by a large difference than the PNFs as observed in Table III, which indicates the improved basic character of functionalized surface. This can be attributed due to the hydroxyl and aldehyde functional groups introduced onto the surface through covalent bonding between glutaraldehyde and PAni. The concept of possible covalent bonding between glutaraldehyde and amine groups of PAni is more evident from the enhancement in acid-base component of surface energy, which signifies proton and electron donating character of surface as discussed in **Section 3.4.**

The enhancement in total surface energy value along with polar components specifically Lewis base component value after surface functionalization is correlated to the biocompatibility assessment of surface functionalized samples in the following sections.

4.5 Fluorescence enhancement of SF-PNFs in presence of aromatic amino acids

4.5.1 Absorption & emission spectroscopy

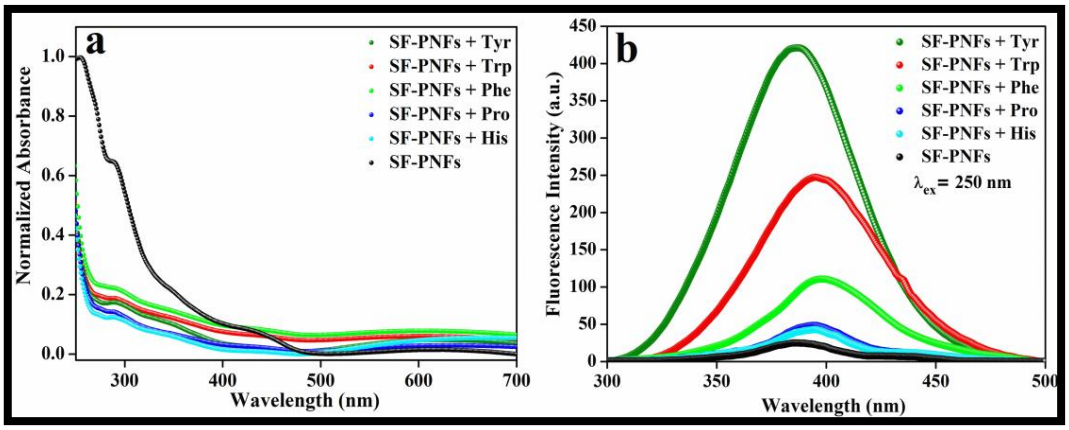

Figure 4.17. (a) UV-Visible absorption spectra and (b) Fluorescence spectra of SF-PNFs before and after exposure to aromatic amino acids Tyrosine (S1), Tryptophan (S2), Phenylalanine (S3), Proline (S4) and Histidine (S5) in PBS at p^H = 7.4.

The features of electronic structures and relative conformational changes of SF-PNFs before and after treating with five aromatic amino acids along with PNFs in 0.1 M PBS at p^H=7.4 are probed by UV-Visible absorption spectroscopy as shown in **Figure 4.17 (a)**. The broad absorption band around 300 nm appeared in the absorption spectrum SF-PNFs, is assigned to the π–π^* band transitions. After treatment with the aromatic amino acids, this peak is slightly blue shifted to 290 nm. The peak at 600 nm associated with quinoid units is observed to be suppressed after treatment of SF-PNFs with aromatic amino acids.

Both PNFs and SF-PNFs exhibit a distinct photoluminescence peak at 385 nm as shown in inset of **Figure 4.17 (b)**. However, the intensity of the peak of SF-PNFs is observed to be higher than the PNFs. It has been observed that when the aromatic amino acids [shown in **Figure 4.18**]are added to the solution of SF-PNFs in PBS, fluorescence response of S1, S2 and S3 is significantly enhanced in comparison to S4 and S5 as observed from **Figure 4.17 (b)**. Enhancement of fluorescence intensity of S1, S2 and S3 can be ascribed to the aromaticity and conjugated double bond present in the system as well as increase in/incorporation of oxygenated species in presence of

the aromatic amino acids [360-362]. Fluorescence intensity of SF-PNFs increases in presence of aromatic amino acids due to low energy π–π^* transitions as a consequence of aromaticity and conjugated double bond present in the system as well as increase in oxygenated species as in Tyrosine. However, in presence of Histidine and Proline, it is low due to the presence of nitrogen in heterocyclics, as the lowest energy transition is involved in n–π^* system, which yields low fluorescence [360-362]. Fluorescence enhancement of PAni after functionalization with glutaraldehyde as well as in presence of aromatic amino acids can also be ascribed to increase in substitution of PAni chain by functional oxygenated species like CHO, OH and aromatic conjugated systems through glutaraldehyde cross linking.

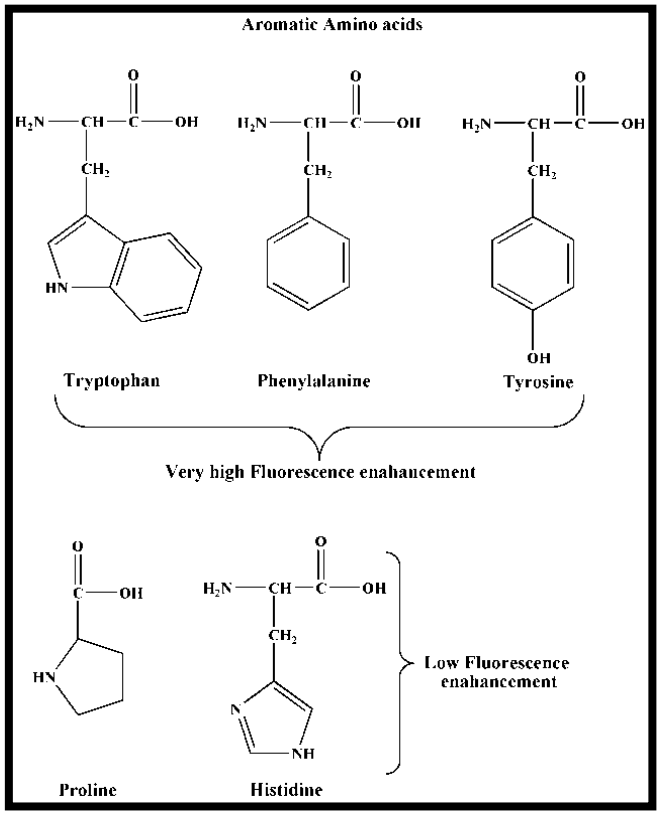

Figure 4.18. Chemical structure of five aromatic amino acids classified in accordance with their contributions to fluorescence enhancement of SF-PNFs.

Though Proline and Histidine do not show fluorescence intrinsically as compared to other three, they contribute to fluorescence enhancement of SF-PNFs to a small extent. Hence, we can't expect resonance energy transfer between SF-PNFs with Proline and Histidine. On the other hand, Tyrosine has intrinsic fluorescence due to its

bond conjugation and aromatic ring and hydroxyl group (-OH) associated with the ring as shown in **Figure 4.18** [368-370]. Tyrosine is also more fluorescent than Tryptophan in solution but in protein, it often quenched due to energy transfer with nearby Tryptophan residues [368, 369]. Tryptophan has intrinsic fluorescence due to its indole group, a dominant UV absorber and emitter in protein [368, 369]. Phenylalanine with a benzene ring and methylene group as shown in **Figure 4.18** is weakly fluorescent only in absence of Tyrosine and Tryptophan in protein [367, 368].

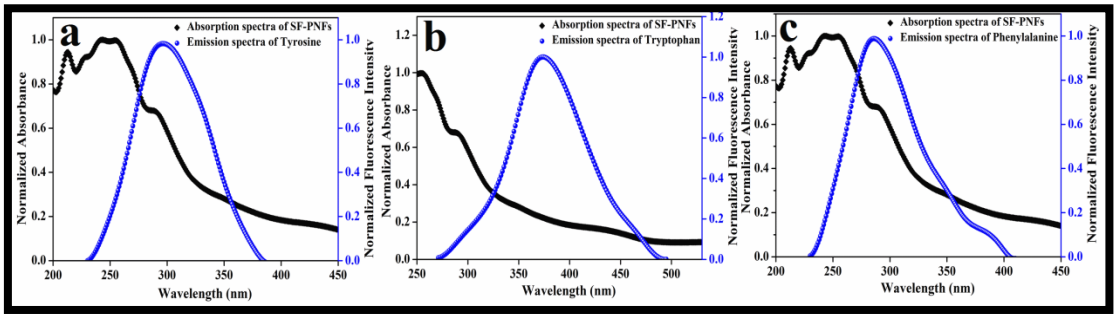

Figure 4.19. Overlapping of absorption spectrum of SF-PNFs (acceptor) with emission spectrum of (d) Tyrosine (donor), (e) Tryptophan (donor) and (f) Phenylalanine (donor) in PBS at $p^H = 7.4$.

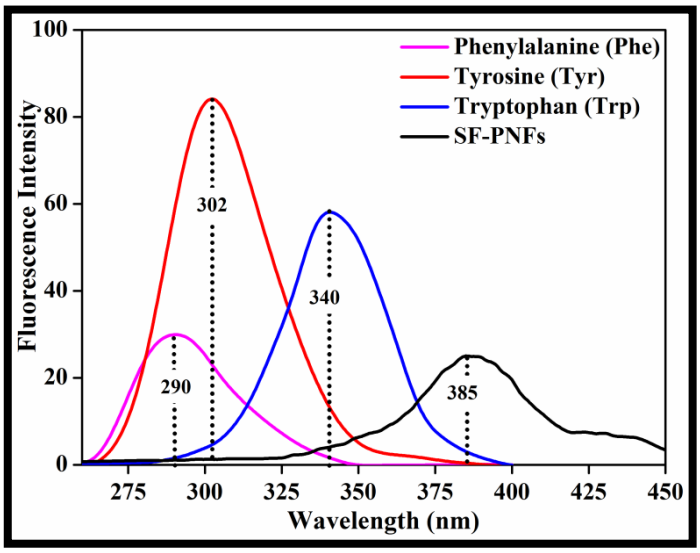

Figure 4.20. Fluorescence spectra of SF-PNFs, Tyrosine, Tryptophan, and Phenylalanine in PBS at $P^H = 7.4$ at an excitation wavelength λ_{ex}= 250 nm.

Fluorescence signal of SF-PNFs in presence of Tyrosine is maximum and minimum in presence of Phenylalanine. As already discussed, both PNFs and SF-PNFs are in

EB form without formation of any polaron band. Therefore, there is no probability of n-π* transition in our case. Several factors like intrinsic fluorescence of the amino acids, bond conjugation, aromaticity and overlapping between absorption spectrum of SF-PNFs and the aromatic amino acids, may lead to higher fluorescence of S1 and S2 than S3.

Emission spectra of Tyrosine, Tryptophan, and Phenylalanine are shown in **Figure 4.20**. FRET occurs when emission spectrum of donor overlaps with the absorption spectrum of acceptor provided donor and acceptor molecules are in close proximity to each other [360]. According to FRET mechanisms, fluorescence enhancement is more probable when absorption spectrum of acceptor and emission spectrum of the donor overlaps substantially giving rise to dipole dipole interaction arises from different polarity of the functional groups present in donor and acceptor [360]. Similar interactions are also predicted in our case as the SF-PNFs and the aromatic amino acids contain polar functional groups like hydroxyl (-OH), aldehyde (-CHO), amino ($-NH_2$) groups. Good spectral overlapping between the absorption spectrum of SF-PNFs with the emission spectra of Tyrosine, Tryptophan, and Phenylalanine is observed as shown in **Figure 4.19 (a-c)**, which indicates that SF-PNFs acts as an acceptor and get excited itself at emission wavelength of these three aromatic amino acids, which act as donor. Thus, fluorescence enhancement of S1, S2 and S3 is also supported by the overlapping of the absorption spectra of SF-PNFs with the emission spectra of Tyrosine, Tryptophan, and Phenylalanine. Moreover, the peak observed at 385 nm in SF-PNFs is found to be red shifted to 389-397 nm region after exposure of SF-PNFs with amino acids Tyrosine (389 nm), Tryptophan (394 nm), Phenylalanine (397 nm), Proline (394 nm) and Histidine (393 nm) as shown in **Figure 4.18**. These spectral shifts observed in absorption and fluorescence spectra of SF-PNFs after treatment with amino acids can be assigned to the binding or interaction between SF-PNFs and the amino acids. Interaction mechanisms between SF-PNFs with Tyrosine, Tryptophan. and Phenylalanine have been investigated by FT-IR and ^{1}H NMR spectroscopy and discussed in the subsequent sections.

4.5.2 FT-IR spectroscopy

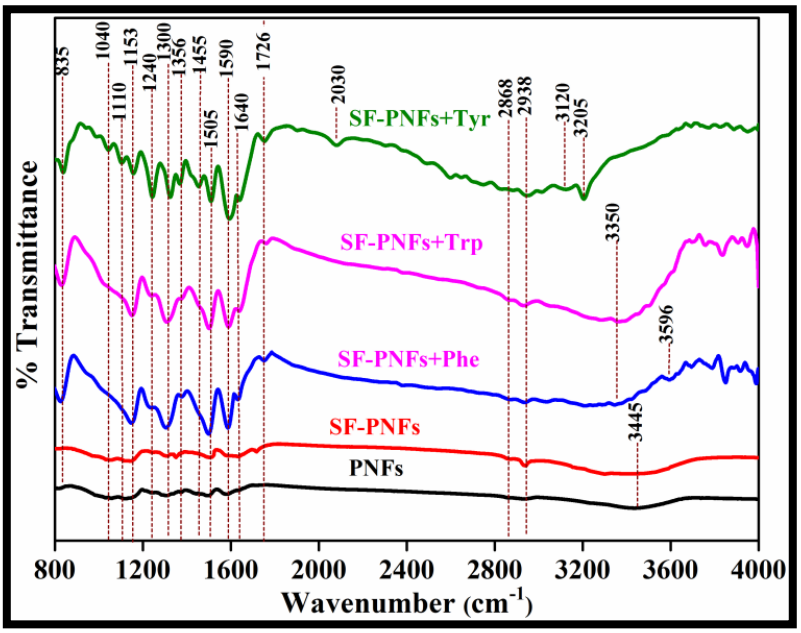

Figure 4.21. Vibrational spectra of PNFs, SF-PNFs and SF-PNFs before and after exposure to Tyrosine (S1), Tryptophan (S2) and Phenylalanine (S3) indicating different covalent interactions between the amino acids and SF-PNFs.

Figure 4.21 displays the comparison among the vibrational spectra of pristine PNFs, SF-PNFs and SF-PNFs with aromatic amino acids namely Tyrosine, Tryptophan, and Phenylalanine to elucidate the interaction mechanisms between SF-PNFs and amino acids. The broad vibrational bands around 3445 cm^{-1} observed in both PNFs and SF-PNFs are attributed to N-H stretching vibration in aromatic amine of PAni [349-352]. However, this broad band has been observed to be expanded to the lower frequency region with a small hump in SF-PNFs can be assigned to secondary N-H stretching vibration in amide indicating the linkage of glutaraldehyde with PAni chains through amide bond formation. It is also possible that broadening of this band with slight shifting to higher frequency region also occurs due to the overlapping of free O-H stretching vibration of cyclic hemiacetal and oligomeric form of glutaraldehyde in SF-PNFs [352]. The broad vibrational bands around 3300 cm^{-1} observed in SF-PNFs when exposed to Tyrosine, Tryptophan, and Phenylalanine are ascribed to hydrogen bonded O-H stretching vibrations overlapped with N-H stretching vibration of secondary amide. The doublet appears at 2886 and 2938 cm^{-1} in SF-PNFs before and

after exposure to amino acids, associated with C-H stretching for aldehyde almost certainly indicates the presence of aldehyde in these complexes. This doublet allows distinguishing aldehyde from carboxylic acid. A small band observed at 1726 cm^{-1} in SF-PNFs in presence of amino acids can be attributed simultaneously to C=O stretching vibration of carboxylic acid and aldehyde [352]. The distinction of carboxylic acid can be confirmed from hydrogen bonded O-H stretching vibrations extended from 2400-3400 cm^{-1} in the vibrational spectra of SF-PNFs in presence of amino acids [352]. The weak but broad absorption band at 1640 cm^{-1} of PNFs and SF-PNFs is attributed to C=N aromatic stretching vibrations in quinoid units [349-351]. This can be simultaneously attributed to C=O stretching vibrations in amide bond and C=N stretching vibrations in Schiff base formed between aldehyde group of monomeric glutaraldehyde in SF-PNFs and amino group of aromatic amino acids. The strong absorption bands, appearing at 1590 cm^{-1} in the vibration spectra of PNFs and SF-PNFs are assigned to C=C stretching vibration of quinoid units of PAni [349-351]. This strong band is often overlapped with N-H bending of secondary amide [352]. The appearance of vibrational bands in the region 1456-1505 cm^{-1} PNFs is due to characteristics C=C stretching vibrations of benzenoid units in PAni [349-351]. The weak peaks of SF-PNFs in the range 1240-1356 cm^{-1} have been observed to be evolved as three strong bands at 1240, 1300 and 1356 cm^{-1}, respectively, in the spectra of SF-PNFs with amino acids [352]. The weak peak around 1350 cm^{-1} assigned to C-N stretching vibrations of aromatic amine in PNFs has been observed to be upshifted to 1356 cm^{-1} in the spectra of SF-PNFs and SF-PNFs in presence of aromatic amino acids, which is attributed to combination of C-N stretching and C-O-H bending vibrations [352]. The sharp splitting and shifting of these two peaks in SF-PNFs to lower wavenumber region 1304-1354 cm^{-1} with increase in intensity indicates possible interaction of cyclic hemiacetal forms of glutaraldehyde with amine and imine sites of PNFs through covalent bonding. The strong band at 1300 cm^{-1} of SF-PNFs in presence of amino acids is attributed C-O stretching vibrations of carboxyl group of amino acids [352]. The band appeared at 1240 cm^{-1} in SF-PNFs in presence of Tyrosine, Tryptophan, and Phenylalanine, is attributed to C-N stretching vibration indicating strong covalent bonding between SF-PNFs with amino acids [352]. However, the intensity of this band is more in presence of Tyrosine. The intense band at 1153 cm^{-1} in SF-PNFs in presence of amino acids is assigned to C-N stretching vibration of aliphatic amine present in amino acids [352]. The strong

absorption band seen at 835 cm^{-1} due to out of plane C-H bending vibrations of SF-PNFs in presence of amino acids indicates an increase the of degree of oxidation of para-disubstituted benzene after functionalization.

4.5.3 ^{1}H NMR spectroscopy

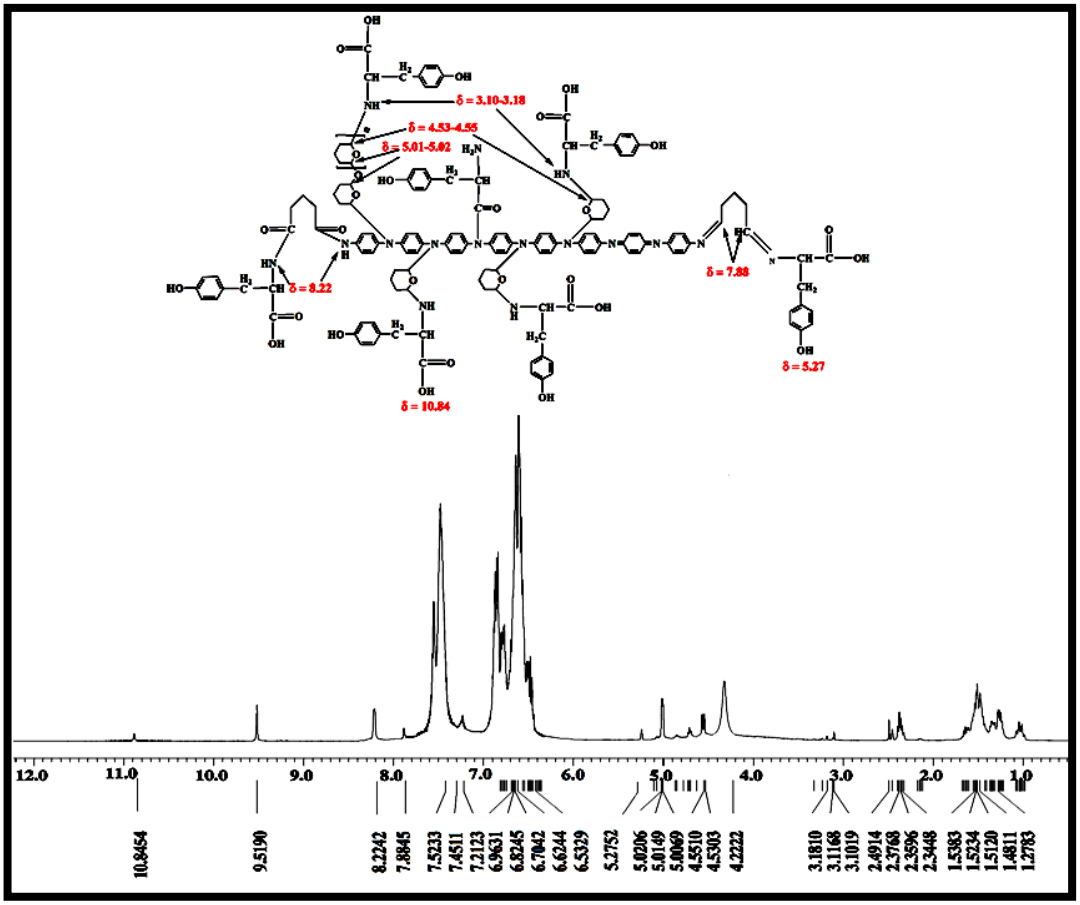

Figure 4.22. ^{1}H NMR spectrum of SF-PNFs in presence of Tyrosine (S1) in DMSO. Observed peaks are assigned by labelling with the help of predicted chemical structure of the polymer amino acid complex.

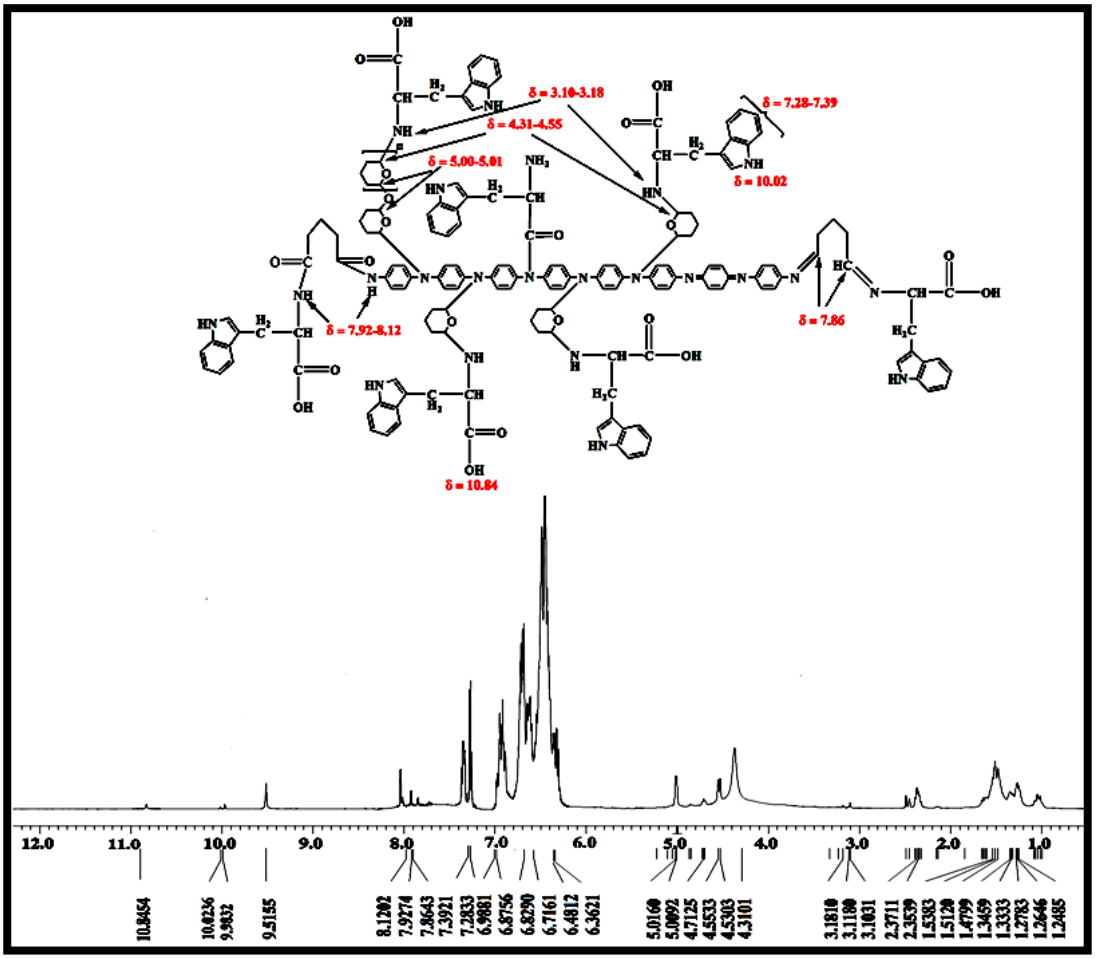

Figure 4.23. ^{1}H NMR spectrum of surface functionalized PAni nanofibers (SF-PNFs) in presence of Tryptophan (S2) in DMSO. Observed peaks are assigned by labelling with the help of predicted chemical structure of the polymer amino acid complex.

^{1}H NMR spectra of PNFs and SF-PNFs have been provided in **Figure 4.12** & **Figure 4.13**. Deprotonation of PAni chains after functionalization is referred by the upfield shifting of the ^{1}H NMR signals in the range 6.90-7.30 ppm due to the aromatic protons of PAni chains as compared to PNFs [353-355]. The signals due to the protons in the benzenoid units of PAni chains are found to be upshifted upto 6.52, 6.31 and 6.29 ppm for S1, S2 and S3, respectively than as compared to SF-PNFs as shown in Figure 5, 6 & 7.

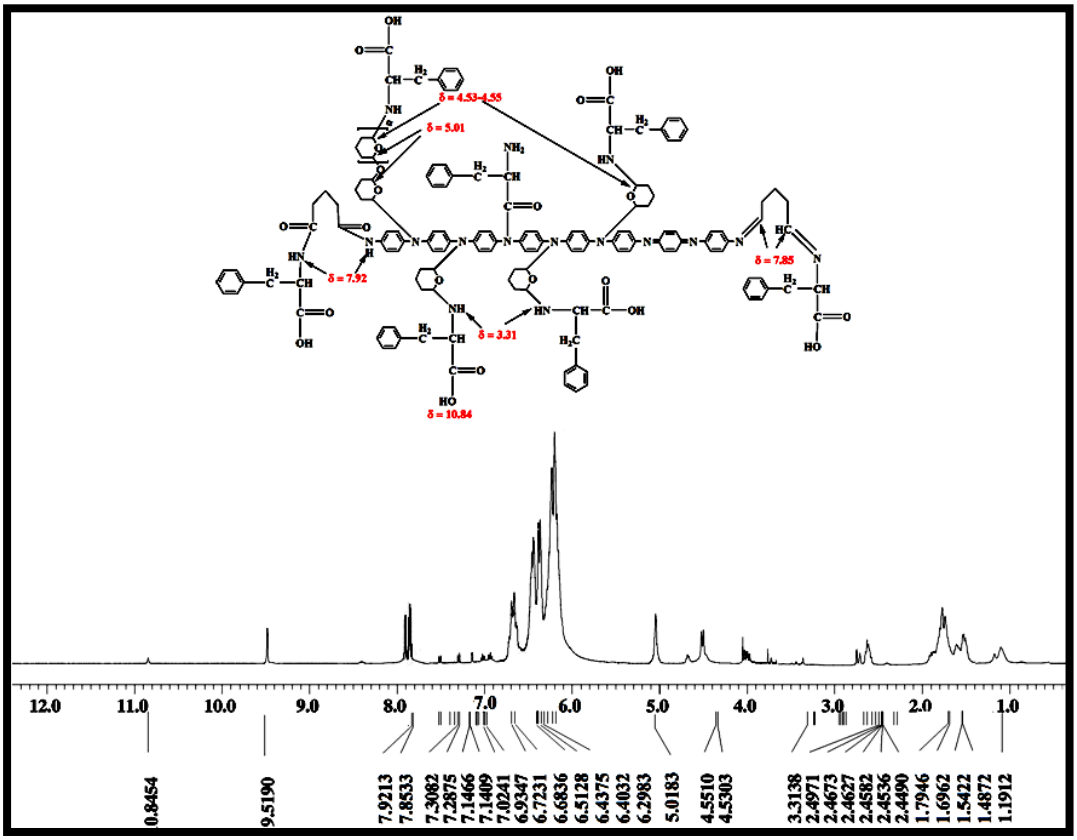

Figure 4.24. ^{1}H NMR spectrum of surface functionalized PAni nanofibers (SF-PNFs) in presence of Phenylalanine (S3) in DMSO. Observed peaks are assigned by labelling with the help of predicted chemical structure of the polymer amino acid complex.

It indicates further deprotonation of the PAni chains due to loss of hydrogen at secondary amine sites of PAni through tertiary amide bond formation between carboxylic group (-COOH) of amino acids and secondary amine (-NH) of PAni. It is further revealed by the appearance of very weak peak around 4.71 ppm in S1, S2 and S3, is attributed to the proton in the secondary amine of PAni chains attached with benzenoid units, which remain unutilized during functionalization by glutaraldehyde [353-355, 371, 372]. The decrease in intensity of this signal with unprotonated secondary amine (-NH) as compared to pristine PNFs and SF-PNFs indirectly indicates the oxidation [loss of hydrogen as shown in **Figure 4.15**] of the secondary amine within the polymer chain during the conjugation with carboxylic group of amino acid. The weak ^{1}H NMR signal due to methylene proton of monomeric glutaraldehyde in the Schiff base formed as a result of interaction between SF-PNFs

and the amino acids has been observed at 7.88, 7.86 and 7.85 ppm for S1, S2 and S3, respectively [372]. The observed weak but sharp ^{1}H NMR chemical shifts at 8.22 ppm, 7.92-8.12 ppm and 7.92 ppm for S1, S2 and S3, respectively are due to proton in the secondary amine of the amide bond formed between SF-PNFs and the amino acids [352]. The ^{1}H NMR signals in the range 4.22-5.02 ppm appeared in S1, S2 and S3 are assigned to the methylene protons of cyclic hemiacetal and oligomeric form of cyclic hemiacetal form of glutaraldehyde attached to one or two oxygen atoms [352, 373]. The signals at 5.01-5.02 ppm for the methylene protons in which methylene carbon is attached to two oxygen atoms as in oligomeric cyclic hemiacetal form of glutaraldehyde as shown in **Figure 4.22-4.24** have been observed to be slightly shifted towards lowfield region as a result of desheilding caused by electronegative oxygen atoms [352, 373]. The signals observed around 4.22-4.53 are due to methylene proton in which the methylene carbon is attached to one oxygen atom and nitrogen atom of amino group of amino acids [352], while the proton in that covalently linked amino group with SF-PNFs gives the signal in the region 3.18-3.31 ppm for S1, S2 and S3 [373]. Two additional signals appeared in the same region for the protons in the quinoid units of PAni, at 7.28 and 7.39 ppm in for S2, are due to the methylene protons in the indole ring of Tryptophan, whereas the signal for proton of amine in the ring is observed at 10.02 ppm [352]. The weak signal marked at 10.84 ppm for S1, S2 and S3 is due to the proton in the carboxylic group of amino acids [352].

The informations obtained from FT-IR and ^{1}H NMR results have been utilized to predict the interaction mechanisms between SF-PNFs with Tyrosine, Tryptophan, and Phenylalanine in correlation with the Fluorescence spectroscopic analysis as shown in **Figure 4.25**.

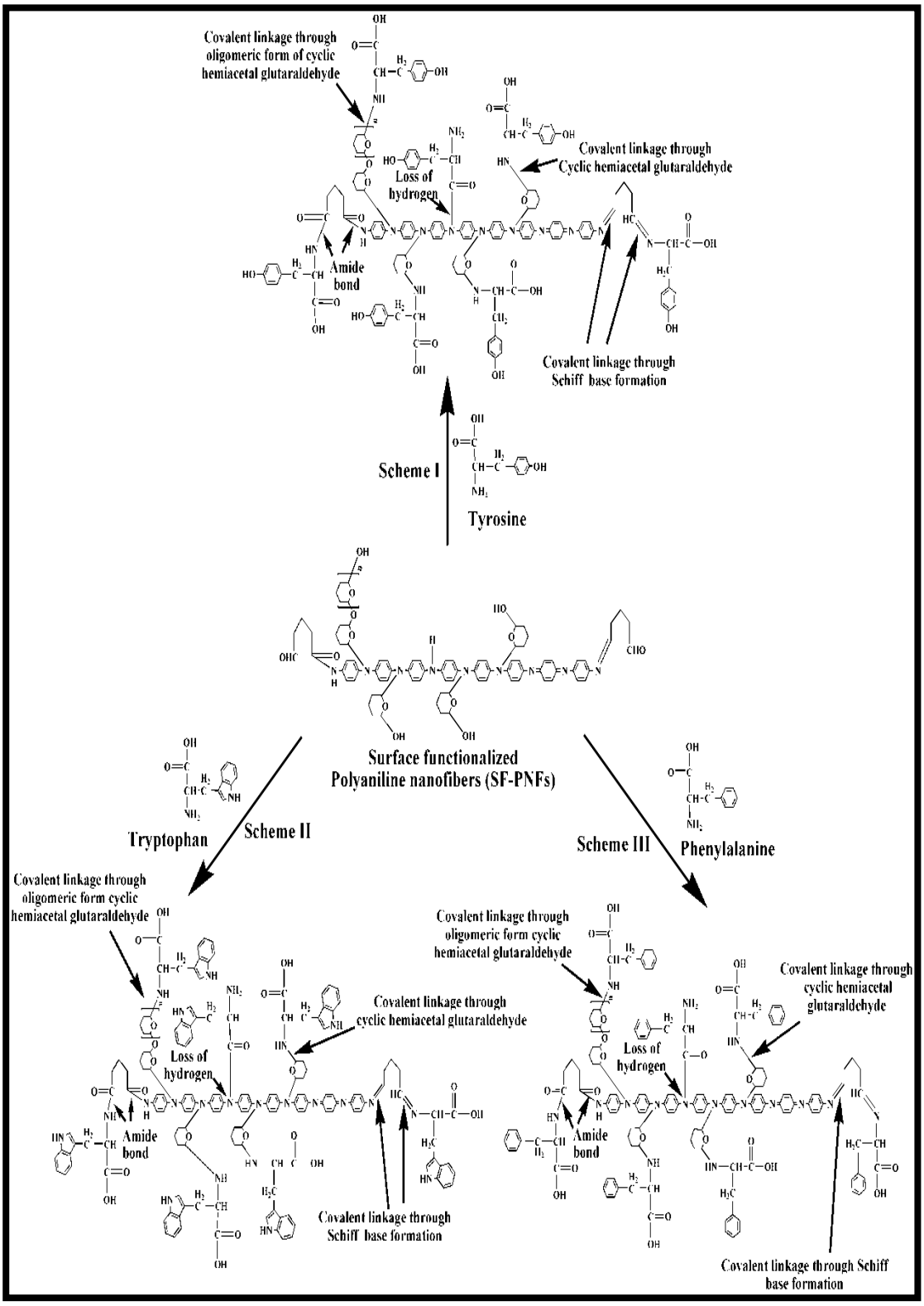

Figure 4.25. Predicted covalent interaction mechanisms between SF-PNFs and Tyrosine (Scheme I), SF-PNFs and Tryptophan (Scheme II) and SF-PNFs and Phenylalanine (Scheme III) based on FT-IR and ^{1}H NMR results.

4.5.4 Study of interaction mechanisms by fluorescence enhancement equation

Fluorescence response curves of SF-PNFs with varying concentrations of Tyrosine, Tryptophan, and Phenylalanine from 5 mM-30 mM are shown in **Figure 4.26 (a-c)**. These fluorescence responses are used to calculate the apparent binding constant (K_A) and number of binding sites (n) of covalently bonded SF-PNFs + Tyr, SF-PNFs+ Trp and SF-PNFs + Phe complexes. The fluorescence micrographs of SF-PNFs before and after exposure to these aromatic amino acids are shown in **Figure 4.27**.

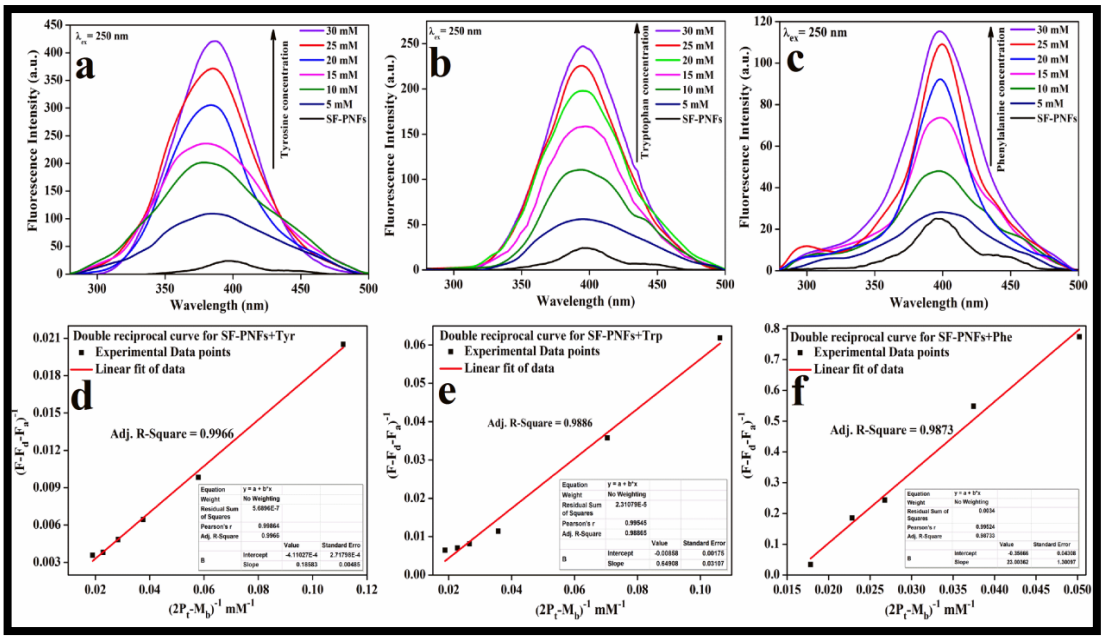

Figure 4.26. Fluorescence response of SF-PNFs when exposed to different concentrations of (a) Tyrosine, (b) Tryptophan and (c) Phenylalanine in PBS at p^H = 7.4. The double reciprocal curves for the interaction between SF-PNFs with (d) Tyrosine (n=2, Adj. R-square = 0.9966), (e) Tryptophan (n=2, Adj. R-square = 0.9886) and (f) Phenylalanine (n=2, Adj. R-square = 0.9873).

The best fitted double reciprocal curves of $[F - F_D - F_A]^{-1}$ against $n[P_t] - [M_b]^{-1}$ for $n=2$ of SF-PNFs + Tyr, SF-PNFs + Trp and SF-PNFs + Phe complexes give apparent binding constant (K_A) values 5.38 X 10^3 M^{-1}, 1.54 X 10^3 M^{-1} and 4.34 X 10^1 M^{-1} , respectively. The K_A value is found to be highest for tyrosine and lowest for Phenylalanine with apparent number of binding sites is two. Higher K_A value indicates

higher affinity between the polymer and the amino acid. Our results show that out of three aromatic amino acids, Tyrosine is the most tightly bound to SF-PNFs through covalent bonding as depicted in the possible interaction mechanisms in **Figure 4.25** giving maximum fluorescence. This indirectly indicates that there is more probability of strong covalent interaction between SF-PNFs and Tyrosine through amide bond, Schiff base and carbon-nitrogen bond formation as shown in **Figure 4.25**. It is also supported by FT-IR and ^{1}H NMR results.

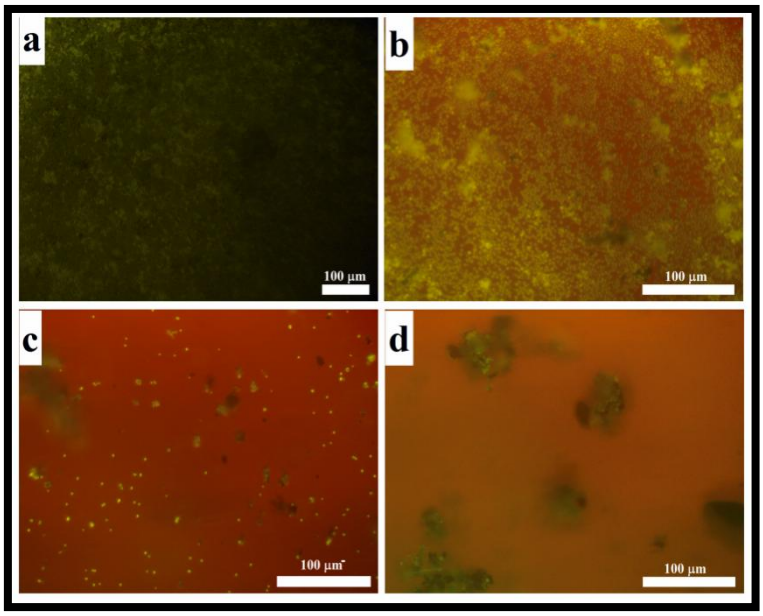

Figure 4.27. Fluorescence micrographs of (a) SF-PNFs before and after exposure to (b)Tyrosine, (b) Tryptophan and (c) Phenylalanine under illumination of 365 nm light acquired by Fluorescence microscope model Leica DM 300.

FRET efficiency (E_{FRET}) has been calculated from the fluorescence quenching of donor (aromatic amino acids) to acceptor (SF-PNFs), which in turn contributes to fluorescence enhancement of SF-PNFs after treatment with the aromatic amino acids (donor) using the following formula [374]:

$$FRET\ efficiency\ (E_{FRET}) = \frac{F_{after} - F_{before}}{F_{after}} \qquad 4.5$$

Where F_{before} = Fluorescence intensity of the amino acid in PBS at p^{H} = 7.4 and F_{after} = Fluorescence intensity of SF-PNFs-amino acid complex in PBS at pH= 7.4.

Table 4.7. FRET Efficiency (E_{FRET}) of SF-PNFs with different concentrations of Tyrosine, Tryptophan, and Phenylalanine. Data are Mean ± S.D.

Amino acid concentrations treated with SF-PNFs	FRET Efficiency (E_{FRET}) %		
	Tyrosine	Tryptophan	Phenylalanine
5 mM	51.02 ± 3.4	48.57 ± 5.21	14.32 ± 1.3
10 mM	73.61 ± 2.74	59.96 ± 5.04	23.82 ± 3.05
15 mM	79.11 ± 4.1	65.55 ± 3.25	43.27 ± 1.85
20 mM	82.02 ± 2.53	69.51 ± 3.43	53.68 ± 2.77
25 mM	85.93 ± 1.65	71.37 ± 2.8	64.94 ± 4.03
30 mM	86.65 ± 2.53	72.79 ± 2.09	67.90 ± 3.13

It has been found that the E_{FRET} is highest for SF-PNFs + Tyr, (acceptor/donor) complex than as compared to SF-PNFs + Trp and SF-PNFs + Phe complexes. The E_{FRET} increases with the concentration of the amino acids in the complexes with SF-PNFs. Maximum E_{FRET} of 86.65%, 72.79% and 67.90% is obtained for 30 mM of Tyrosine, Tryptophan, and Phenylalanine with SF-PNFs, respectively [**Table 4.7**]. High values of E_{FRET} are supported by the overlapping between the absorption spectrum of acceptor and emission spectrum of donor as in discussed in **Section 3.2**. The stronger affinity or tight binding between SF-PNFs and Tyrosine than that of the other two aromatic amino acids as revealed by the highest K_A value for this complex, allows both SF-PNFs and Tyrosine to be in close proximity, which is necessary for energy transfer. FRET efficiency of SF-PNFs with Proline and Histidine can't be calculated as no significant fluorescence was observed for them in PBS.

4.5.5 Comparative interference study

As human body may contain other amino acids such as Alanine, Arginine, Asparagine, Aspartic acid, Cysteine, Isoleucine, Glutamic acid, Leucine, Methionine, Serine, Threonine and Valine, those can interfere with fluorescence response of SF-PNFs with aromatic amino acids: Tyrosine, Tryptophan, and Phenylalanine. Therefore, comparative interference study has also been performed with SF-PNFs when treated with fourteen other amino acids along with Tyrosine, Tryptophan, and Phenylalanine, in terms of relative fluorescence response as shown in **Figure 4.28**.

Besides these, comparative interference study of fluorescence response of pristine PNFs when treated with Tyrosine, Tryptophan, Phenylalanine, Proline and Histidine has been carried out as shown **Figure 4.28**. It is quite evident from this study that all the amino acids except Serine, Proline and Histidine showed negligible response even at concentration of 30 mM as compared to three aromatic amino acids. Results indicates that Serine, Proline and Histidine showed minute response as compared to the response shown by three aromatic amino acids. The amino acids other than Tyrosine, Tryptophan, and Phenylalanine are known to lack of intrinsic significant fluorescence properties [360, 368, 369]. Therefore, there is no possibility of energy transfer between SF-PNFs and those amino acids during interaction between them causing no fluorescence enhancement. Due to the lack of glutaraldehyde cross-linking, covalent interaction between pristine PNFs with Tyrosine, Tryptophan, and Phenylalanine is not generally expected due to hydrophobic nature of PAni. Hence, in spite of the overlapping between the absorption spectrum of PNFs and emission spectra of the three aromatic amino acids, no fluorescence enhancement was observed as in the case of SF-PNFs.

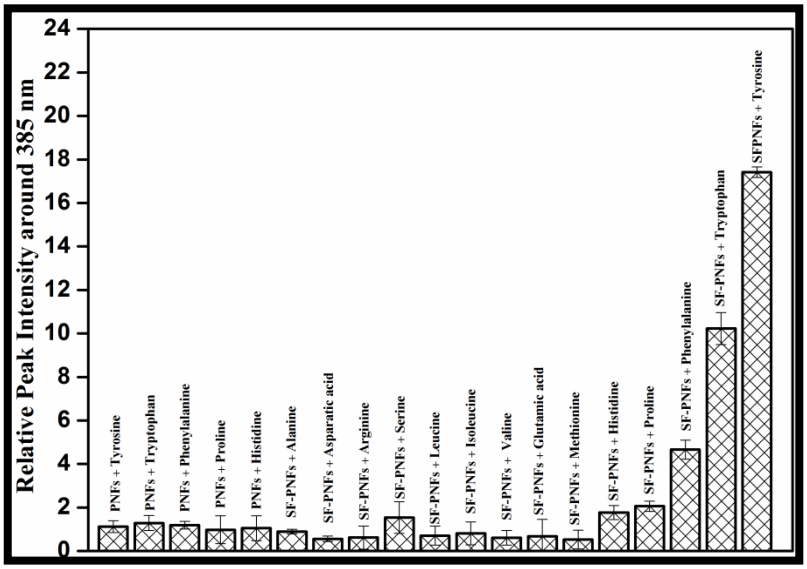

Figure 4.28. Comparative interference studies using different amino acids with both PNFs and SF-PNFs in PBS at pH = 7.4. The concentration of PNFs and SF-PNFs kept fixed throughout the experiment, while the concentration of all the amino acids is taken as 30 mM.

4.6 Biological characterization

4.6.1 Hemolysis activity

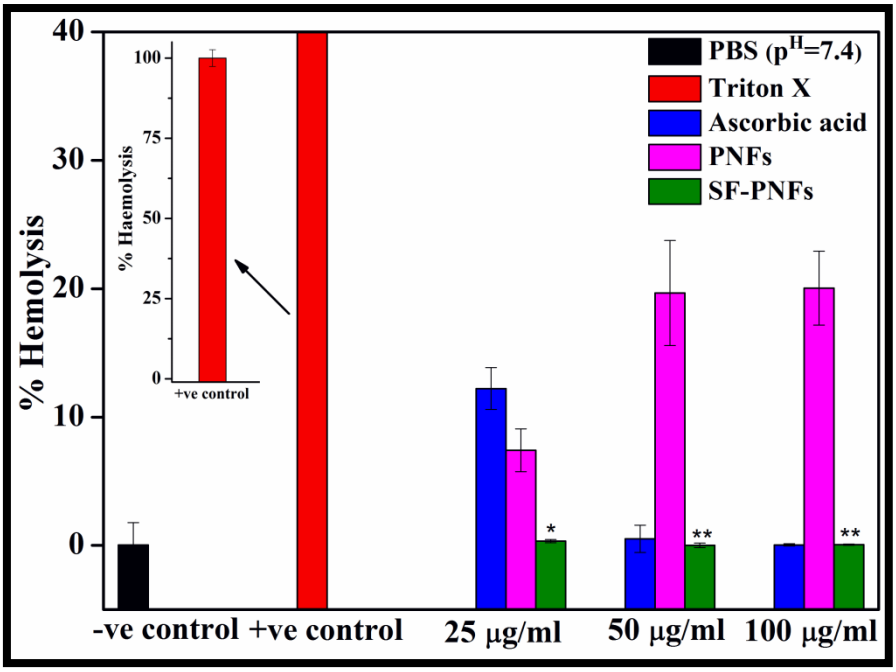

Figure 4.29. Hemolysis activity of PNFs and SF-PNFs in terms of percentage of hemolysis in PBS at pH=7.4 showing a comparison of hemolysis activity of drug ascorbic acid. Data are expressed as means ± SD, n=3; **: P≤0.001, values are significantly different from those obtained with +ve control.

It has been observed that SF-PNFs show significantly very less hemolysis as compared to the pristine samples as shown in **Figure 4.29**. The surface functionalized samples are found to exhibit hemolysis activity less than one percentage and hence, they are non-hemolytic. The percentage of hemolysis of all the samples is compared with the hemolysis activity of ascorbic acid, also known as Vitamin C. Ascorbic acid is an organic compound having tremendous antioxidant properties, which potentially reduces the oxidative stress and thereby, protects red blood cells (RBCs) from rupturing. More interestingly, SF-PNFs are also found to exhibit hemolysis activity very similar to the ascorbic acid in presence of Triton X-100, which is generally used to lyse cells to extract protein or organelles, or to permeabilize the membranes of living cells. Therefore, this observation reveals that surface functionalization of PNFs

renders stability towards cell membrane. Not only this, it also indirectly indicated to the improved antioxidant property of SF-PNFs. However, antioxidant property of PAni is quite expected as several researchers have already reported this property of PAni [375, 376]. But, it is important to note in this work that enhancement of membrane stability property as well as antioxidant property of SF-PNFs is caused only by surface functionalization by glutaraldehyde and it is clearly seen from **Figure 4.29**, when compared with the hemolysis activity of pristine PNFs.

4.6.2 MTS proliferation assay

The MTS results shown in **Figure 4.30** suggest that pure PAni nanofibers are more cytotoxic than SF-PNFs, indicating surface functionalization by glutaraldehyde has played a critical role in determining the biocompatibility of the material. The percent of MDA-MB-21 assessed after 24 h of culture is significantly greater on SF-PNFs, when compared to PNFs ($p \leq 0.05$). Although biocompatibility of PAni had been reported earlier, the lower cell viability on PAni film, in the case, is attributed to the lack of proper binding sites, which is necessary for favourable cell-biomaterial interactions.

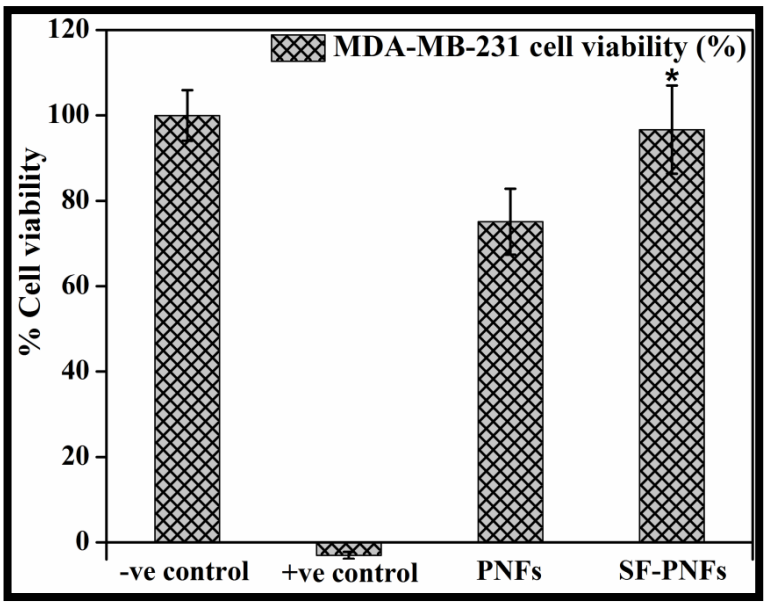

Figure 4.30. Percentage of MDA-MB-231 cell viability on films of PNFs and SF-PNFs in direct contact after 24 h of culture as compared to tissue culture plastic (TCP) as a negative control and tert butyl maleate as a positive control. Data were Mean ± S.D, n=3.$^{*} \leq 0.05$.

In normal cell mechanisms, protein adsorption is the determining step in the first phase during cell biomaterial interaction for controlling cell viability. Moreover, the type of adsorbed protein layer and their orientations are related to the surface properties especially to surface energy [377]. It has been also proved that the polar component of surface energy and Lewis basicity play a key role in interfacial interactions between cell and biomaterials leading to surface biocompatibility [378]. Although, the very low and very high values of these components are not suitable for cellular activities, the values reported in this work are found to be quite utile for improved cell viability on SF-PNFs, which nearly equal to the negative control (TCP). Thus, the improved cell viability can be strongly correlated with the results obtained by FT-IR, NMR techniques as well as surface energy calculations. The results indicate the potential of SF-PNFs in tissue engineering applications.

4.6.3 Acridine orange/ethidium bromide (AO/EtBr) staining

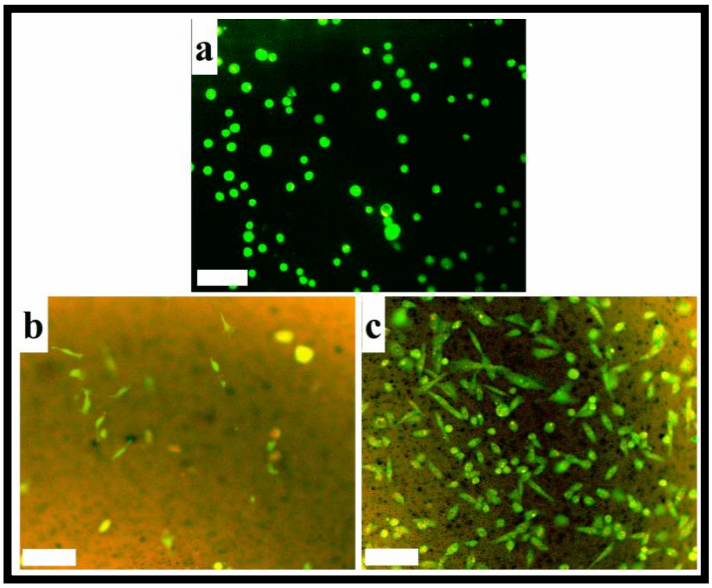

Figure 4.31. Acridine orange/ethidium bromide (AO/EtBr) stained fluorescence images of MDA-MB-231 cells cultured for 48 h on (a) glass cover slip, (b) PNFs and (c) SF-PNFs (Scale bar = 75μm).

For quantitative analysis of cell morphology and spreading, MDA-MB-231 cells cultured on the films of PNFs and SF-PNFs were stained with acridine orange/ethidium bromide (AO/EtBr) after 48 h of culture. AO emits green fluorescence and red fluorescence upon binding with double-stranded DNA (dsDNA)

and to single-stranded DNA (ssDNA) or RNA, respectively. AO is an intercalating dye that can permeate both live and dead cells. Since, it is a cationic dye, it can also penetrate acidic compartments such as lysosomes at low pH level and emit orange fluorescence. Ethidium bromide (EtBR), a membrane-impermeable dye is taken up only by cells with a compromised cell membrane and emits red fluorescence on intercalation into DNA. The fluorescence micrographs of AO/EtBr stained MDA-MB-231 cells on the non-functionalized and glutaraldehyde functionalized PAni nanofibers films along with glass cover slip after 48 h of culture are shown in **Figure 4.31**. The cells on the SF-PNFs emit relatively bright green fluorescence as compared to those on the PNFs. The staining can be visualized throughout the cell bodies cultured on all the scaffolds.

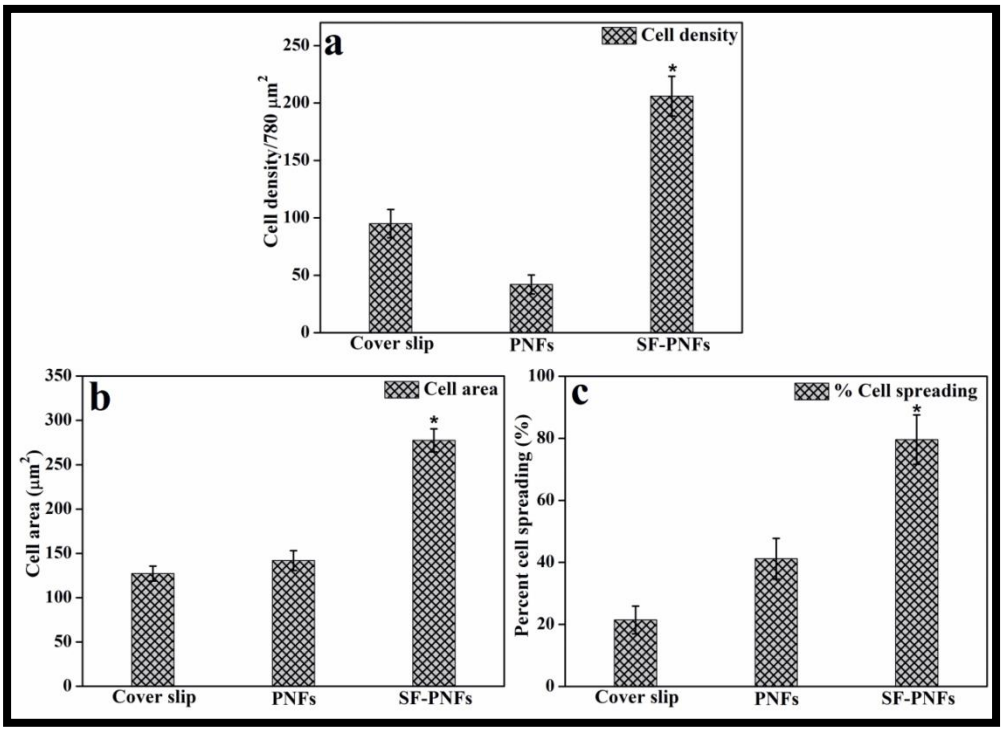

Figure 4.32. Quantitative analysis of (a) cell density per 780 μm^2 area,(b) projected cell area and (c) percent of cell spreading, derived from the AO/EtBr stained fluorescence images of MDA-MB-231 cells after 48 h of culture. Data were expressed as Mean ± S.D, n=6.*indicates statistically significance difference at ≤0.05.

The fluorescence micrographs shows that the cells cultured on glutaraldehyde functionalized PAni film, i.e., SF-PNFs, possess elongated or polygonal shape with higher cell counts [**Figure 4.31 (b)**], while the cells cultured on the non-functionalized PAni films, i.e., PNFs, possess round morphology with lower cell counts [**Figure 4.31 (a)**]. This observation reveals healthier cell morphology on SF-PNFs than that of PNFs. For quantitative analysis of cell density, cell morphology and spreading, the respective fluorescence micrographs of acridine orange stained cells were processed in ImageJ software and the results are depicted in **Figure 4.32 (a-c)** in terms of cell counts, area covered by each cell and percentage of cell spreading. Morphological analysis was limited to the cells, which were not in physical contact with more than one cell. The cells that adopted elongated, polygonal shape, with filopodia- or lamellipodia-like extensions were regarded as spreading cells. In contrast, the cells that retained round morphology were regarded as nonspreading cells. Cell spreading was evaluated in terms of percent of spreading by dividing the number of spread cells by the total number of bound cells but with round morphology. To ensure a representative count or measurement, each sample was divided into quarters and two fields per each quarter were photographed. All the experiments were repeated for six times. The cell density on SF-PNFs film (206 ± 17) is significantly higher than that counted on PNFs film (42 ± 9) and control glass cover slip (95 ± 12), at ≤ 0.05 [**Figure 4.32 (a)**]. Each of MDA-MB-231 cells cultured on SF-PNFs (277 ± 13 μm^2) covers larger area than the area covered by each cell on PNFs (141 ± 11 μm^2) and control glass cover slip (127 ± 8 μm^2) [**Figure 4.32 (b)**]. The difference in area covered by each cell on these substrates is statistically significant at $p \leq 0.05$. Furthermore, the percentage of cell spreading on SF-PNFs (79% ± 8) is also significantly higher than that of the PNFs (41% ± 7) and control glass cover slip (21% ± 5) at $p \leq 0.05$ [**Figure 4.32 (c)**]. The results suggest that surface functionalization of PAni nanofibers by glutaraldehyde has significant impact in the modulation of cellular activities on the PAni nanofibers based scaffold. The enhanced cell area and cell spreading on the glutaraldehyde functionalized PAni nanofibers is attributed to the incorporation aldehyde (CHO) and hydroxyl (OH) groups on the surface after surface functionalization leading to favorable cell-biomaterial interaction.

4.5.4 Cell adhesion test

SEM of MDA-MB-231 cells cultured on non-functionalized and glutaraldehyde functionalized PAni nanofibers films, i.e., PNFs and SF-PNFs were accomplished to confirm the cell attachment and the results are presented in **Figure 4.33**. SEM of MDA-MB-231 cells grown on SF-PNFs reveals good attachment with the substrate with visible cytoplasmic extensions [**Figure 4.33 (b1 & b2)**]. In contrast, MDA-MB-231 cells poorly attach to the non-functionalized PNFs with irregular morophology [**Figure 4.33 (a1 & a2)**]. In fact, SEM confirms the AO/EtBr staining results.

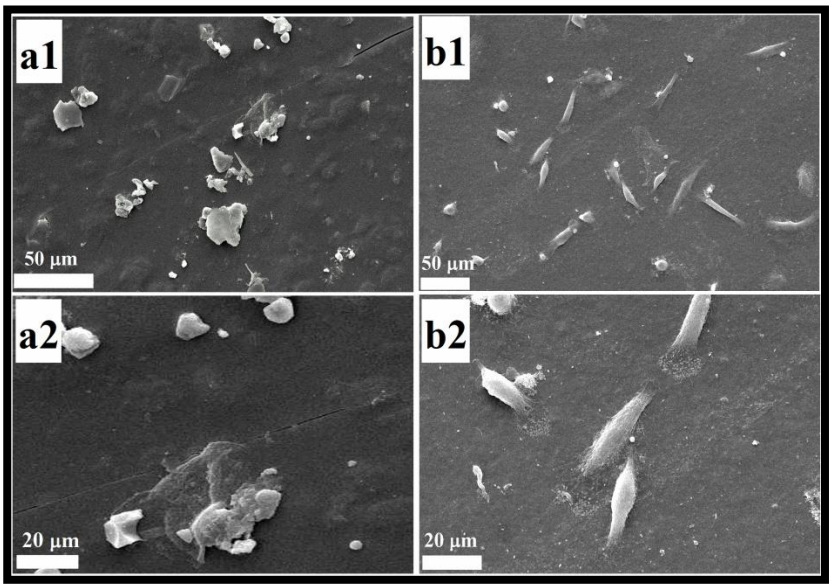

Figure 4.33. Scanning electron micrographs of MDA-MB-231 cells on PNFs (a1 & a2) and SF-PNFs (b1 & b2) after 48 h of culture at lower magnification (a1: 500X, b1:300X) and higher magnification (b1 & b2: 900X).

4.7 Summary

Herein, we have shown the synthesis of PAni nanofibers (PNFs) with average diameters of 35.66 nm without using any organic solvent by dilute polymerization method, as confirmed by TEM and SEM. PAni nanofibers film has been prepared using NMP as solvent, which has interconnected networks of nanofibers and highly entangled morphology as revealed by SEM. The synthesized PNFs have been surface functionalized by glutaraldehyde to improve the surface hydrophilicity, leading to design a bioactive platform for favorable interaction with biomolecules and living cell system. The study demonstrates the modulation of the various physicochemical and

biological properties of PNFs after surface functionalization by glutaraldehydes, which have been accomplished with the help of various sophisticated analytical tools and assays.

The *I-V* measurement demonstrates that surface functionalization has been without much affecting the conductive properties of PAni nanofibers films as there is only slight increase in the sheet resistance of PNFs after functionalization from 1.23 ± 0.48 × 10^5 Ω.cm (PNFs) to 1.33± 0.55 × 10^5 Ω.cm (SF-PNFs) due to loss of π–π conjugation during functionalization process. Most importantly, PNFs retain their conductive properties in physiological condition when kept in PBS (pH=7.4) for 30 days as revealed by stability test. The mechanical properties such as stiffness constant (*E*) and ultimate tensile strength (UTS) of glutaraldehyde functionalized PAni nanofibers film have been found to be enhanced as revealed by tensile strength test, which is attributed to the cross-linking between the polymer chains after surface functionalization as indicated by the XRD results. The incorporation of polar groups viz. aldehyde (-CHO) and hydroxyl (-OH) functionalities on the surface of the PAni nanofibers has been confirmed by FT-IR and ^{1}H NMR spectroscopy. UV-visible absorption and photoluminescence studies suggest reduction of the quinoid units resulting in greater number of benzenoid units in the PAni chains, after surface functionalization, due to partial reduction at the imine sites by the aldehyde and hydroxyl functionalities of glutaraldehyde, which can be correlated with the FT-IR and ^{1}H NMR results. Surface energy calculations by OWRK and AB method demonstrate up to 6-9% enhancement in surface polarity of the PAni nanofibers after surface functionalization by glutaraldehyde. More specifically, the enhancement in the basic component of surface energy $\left(\gamma_s^-\right)$evaluated by AB method indirectly indicates the introduction basic aldehyde (-CHO) and hydroxyl (-OH) groups on the surface of PNFs after surface functionalization.

One of the important findings of this study is the enhancement in fluorescence signal of SF-PNFs than that of PNFs. Therefore, taking the advantages of enhanced hydrophilicity and fluorescence signal, fluorescence spectroscopy has been used as an analytical tool with SF-PNFs as a substrate to monitor any biochemical reactions involving three aromatic amino acids viz. Tyrosine (Tyr), Tryptophan (Trp) and Phenylalanine (Phe). Remarkable enhancement in fluorescence signals of SF-PNFs in presence of aromatic amino acids due to good covalent interaction the polymer and

amino acids as revealed by FT-IR and 1H NMR spectroscopy, has been observed and the apparent binding constant (K_A) and the number of binding sites (n) have been calculated using fluorescence enhancement equation. The K_A value has been found to be highest for SF-PNFs+Tyr complex and n is two for all the polymer amino acid complexes, which are in agreement with the FT-IR and 1H NMR results. Fluorescence resonance energy transfer (FRET) efficiency has been found to be highest for SF-PNFs+Tyr complex giving maximum fluorescence enhancement. The study of interaction mechanisms by means of an extremely sensitive technique like fluorescence spectroscopy using SF-PNFs as a substrate may provide a promising analytical tool for detection and monitoring any biochemical reactions involving these three aromatic amino acidsthat are precursors to several proteins like horomones, melanin, thyroid, serotonin, epinephrine etc.

Furthermore, SF-PNFs have been found to be biocompatible as revealed from Hemolysis assay and MTS assay. The surface functionalized samples are found to exhibit hemolysis activity less than 1% and hence, they are non-hemolytic. Fluorescence microscopy of AO/EtBr stained MDA-MB-231 cells shows enhanced cell adhesion, spreading and proliferation on SF-PNFs when compared to PNFs, whereas cell attachment on the PAni scaffold was confirmed by SEM. The enhanced cell adhesion, spreading and proliferation on SF-PNFs suggest favorable cell-biomaterial interactions owing to improved surface hydrophilicity as a result of incorporation of polar hydroxyl and aldehyde functionality after surface functionalization by glutaraldehyde. The results suggest that improved bioactivity and biocompatibility of SF-PNFs can make it a promising candidate for biomedical applications such as tissue engineering and biosensing applications.